ce

optimisation of direct air capture using

a
m
i
n
e
-
f
u
n
c
t
i
o
n
a
l
i
s
e
d

m
e
t
a
l
l
-
o
r
g
a
n
i
c

f
r
a
m
e
w
o

rks

Ayp ecle

dR t

ps://knowledge.lancashire.a

c.uk/id/eprint/57643/
https://doi.org/10.1

0
1
6
/
j
.
s
e
p
p
u
r
.
2
0
2
5
.
1
3
6
1
7
7

,

Maryam,

Nasrianni,

Hamid

Reza,

Khajenoori,

Leila, Rasmussen, Samira Khanian and William

s
,
K
a
r
l
S
(
2
0
2
6
)
S
u
r
r
o
g
a
t
e
-
a
s
s
i
s
t
e
d
c
y
c
l
i
c

performance optimisation of direct air capt

ureusingaminee-functionalisedmetall-organani

c

f
r
a
m
e
w
o
r
k
s
.

S
e
p
a
r
a
t
i
o
n

a
n
d

P
u
r
i
f
i
c
a
t
i
o
n

T

echnology, 383. pp. 136177. ISSN 1383-5866

Nasiri, Shirin, Maryam, Nasrin, Hamid Reza,

Khajenoori, Leila, Rasmussen, Samira Khanji

Separation and Purification Technology 383 (2026) 136177

Contents lists available at ScienceDirect

Separation and Purification Technology

journal homepage: www.elsevier.com/locate/seppur

Surrogate-assisted cyclic performance optimisation of direct air capture using amine-functionalised metal–organic frameworks

Maryam Nasiri-ghiri [a], Hamid Reza Nasriani [a,*], Leila Khajenoori [a], Samira Khani Rasmussen [b], Karl Williams [a]

[a] School of Engineering and Computing, University of Lancashire, Preston PR1 2HE, United Kingdom
[b] Geological Survey of Denmark and Greenland, Department of Geo-Energy and Storage, ØsterVoldgade 10, Copenhagen 1350, Denmark

ARTICLE INFO

Editor name: Z Bao

Keywords:
Direct air capture
Temperature vacuum swing adsorption
CCUS
Artificial neural network
Metal organic framework

ABSTRACT

Direct Air Capture (DAC) using solid sorbents has emerged as a promising technology for achieving net-negative CO_2 emissions and meeting global climate targets. Among the available sorbent materials, amine-functionalised metal–organic frameworks (MOFs) have gained significant attention due to their tuneable structures and strong affinity for CO_2 under ambient conditions. In particular, mmen-Mg_2(dobpdc) has demonstrated exceptional CO_2 uptake capacity, making it a strong candidate for DAC applications. However, its process-level performance optimisation under realistic operating conditions remains insufficiently explored. This study introduces the first comprehensive multi-objective optimisation of a temperature–vacuum swing adsorption (TVSA) process employing the amine-functionalised metal–organic framework mmen-Mg_2(dobpdc) as the sorbent for direct air capture (DAC) of CO_2. The optimisation simultaneously targets minimisation of energy consumption and maximisation of CO_2 recovery and productivity, while ensuring high product purity, thereby providing new insights into the process–material interactions governing DAC performance. To achieve this, a validated dynamic temperature vacuum swing adsorption (TVSA) model was developed in Aspen Adsorption, integrated with a surrogate artificial neural network (ANN) and optimised using the Non-dominated Sorting Genetic Algorithm (NSGA-II). This approach facilitates efficient multi-objective optimisation of key process variables, significantly reducing computational time from approximately 350 days to two hours. The resulting Pareto fronts reveal clear trade-offs between specific energy consumption (SEC), recovery, and productivity at purities above 95 %. The optimised design achieved a 37 % increase in recovery, a threefold improvement in productivity, and a 14.9 % reduction in SEC, at the cost of a modest 3 % decrease in CO_2 purity (from 98 % to 95 %) compared to the base case. Moreover, the study highlights the strong influence of ambient temperature on process performance, showing that mmen-Mg_2(dobpdc) exhibits enhanced CO_2 uptake below 8 °C, demonstrating its suitability for DAC operation in cool climates.

1. Introduction

Atmospheric carbon dioxide (CO_2) concentration over the past three glacial cycles increased from approximately 180 ppm (ppm) to 427.87 ppm as recorded in July 2025 [1], with an average annual growth rate of nearly two ppm [2,3]. This escalation has accelerated global climate change and underscored the urgency of mitigation strategies. To address the Paris Agreement 2015 goals—restricting warming to below 2 °C and ideally 1.5 °C above pre-industrial levels—substantial efforts in decarbonisation are required [4] [5]. While conventional carbon capture, utilisation, and storage (CCUS) technologies are critical components of mitigation strategies, their focus on point sources limits their ability to address dispersed emissions. According to the International Energy Agency (IEA), CCUS could reduce global CO_2 emissions by nearly 20 % and reduce the cost of future climate mitigation by up to 70 % [2,5]. In this context, direct air capture (DAC) has gained attention as a complementary negative emission technology to address both current and historical CO_2 emissions directly from the atmosphere [6,7].

Currently, post-combustion carbon capture can be effectively undertaken through a variety of technologies, including absorption [8,9], adsorption, membrane separation [10], and cryogenic distillation processes [11,12], each encompassing diverse techniques and methodologies [13]. The adsorption process has emerged as a promising alternative

* Corresponding author.
E-mail address: hrnasriani@lancashire.ac.uk (H.R. Nasriani).

https://doi.org/10.1016/j.seppur.2025.136177
Received 16 September 2025; Received in revised form 11 November 2025; Accepted 21 November 2025
Available online 29 November 2025

Nomenclature

T_s	Gas phase temperature (°C)
T_g	Solid phase temperature (°C)
$Y_{predicted}$	Predicted value by ANN
Y_{actual}	Actual value of performance indicators
R^2	Coefficient of determination
AARD	Average absolute relative deviation
RMSE	Root mean squared error
GA	Genetic algorithm
LHS	Latin hypercube sampling
PIs	Performance indicators
PDEs	Partial differential equations

Abbreviations

VSA	Vacuum swing adsorption
PAES	Pareto-archived evolution strategy
MOOPs	Multi-objective optimisation problems
NSGA-II	Non-dominating sorting genetic algorithm
ANN	Artificial neural network
SEC	Specific energy consumption (MJ/kg CO_2)
DAC	Direct air capture
MOF	Metal organic framework
CCUS	Carbon capture, utilisation, and storage
TVSA	Temperature vacuum swing adsorption
RH	Relative humidity
LDF	Linear driving force
S-TVSA	Steam assistance TVSA
PSA	Pressure swing adsorption
TSA	Temperature swing adsorption
SPEA	Strength Pareto EA

to conventional absorption, particularly due to its ability to overcome key limitations such as high solvent degradation, corrosiveness, and substantial energy requirement for solvent regeneration [14,15]. Adsorption processes employ various regeneration methods and are typically classified based on whether regeneration involves altering temperature, pressure, or both. Compared to other separation technologies, temperature vacuum swing adsorption (TVSA) offers several advantages for DAC. By combining elevated temperature and vacuum, TVSA enables higher product purity [16], faster desorption rate compared to temperature swing adsorption (TSA) [17,18], greater working capacity [17], and lower energy consumption than pressure vacuum swing adsorption (PVSA) [19]. A comparative study of TSA, pressure temperature swing adsorption (PTSA), and TVSA cycles using Polyethylene terephthalate (PET)-waste-derived activated carbon reported that the TVSA configuration achieved the highest exergy efficiency (32.9 %), confirming its superior energy utilisation and practical applicability for post-combustion CO_2 capture under moderate feed concentrations (10–20 vol%) [20]. TVSA technology has been successfully applied to amine-functionalised nanocellulose for extracting CO_2 and water vapour from ambient air (10–30 °C, 20–80 % relative humidity (RH)). The process achieves over 94.4 % CO_2 purity, requiring approximately 12.5 kJ/mol CO_2 of mechanical work and 493–640 kJ/mol CO_2 of low-grade heat, depending on humidity [21]. Zhu et al. developed a three-step steam-assisted temperature vacuum-swing adsorption (S-TVSA) cycle based on a packed column for use in DAC systems. The process achieved 4.45 mol/ kg CO_2 day productivity at 0.295 MJ /mol energy demand using low-grade heat (< 100 °C) via steam purging [22].

The performance of any adsorbent is dependent on the specific process configuration including the duration of the adsorption and desorption cycles, as well as the vacuum level and temperature applied during the desorption stage. To accurately assess the suitability and competitiveness of a sorbent, it needs to be evaluated through detailed simulations and standardised optimisation across various process designs [23]. In engineering, many optimisation problems involve simultaneously optimising multiple objectives, known as multi-objective optimisation problems (MOOPs). These problems become particularly challenging when the objectives conflict with one another, meaning that the optimal solution for one objective differs from that of another. When solving such problems, whether constraints or not, the results are typically a set of trade-off optimal solutions referred to as Pareto-optimal solutions [24]. The Non-Dominated Sorting Genetic Algorithm (NSGA-II) was initially proposed by Deb et al. [25] as an efficient multi-objective evolutionary algorithm that introduced a fast non-dominated sorting procedure, an elitist selection mechanism, and a parameter-less crowding distance operator for diversity preservation. Through validation on several benchmark problems, NSGA-II demonstrated superior convergence and solution diversity compared to other contemporary approaches such as Pareto-archived evolution strategy (PAES) [26] and strength Pareto EA (SPEA) [27]. It is a widely applied and effective evolutionary algorithm specifically developed to address MOOPs, providing a Powerful decision-space exploration capabilities based on the principles of Genetic Algorithm (GA). NSGA-II operates based on four key mechanisms: Non-Dominated Sorting, Elite Preserving Operator, Crowding Distance, and the Selection Operator [28]. This algorithm has been extensively applied in engineering for identifying Pareto-optimal solutions in problems involving multiple conflicting objectives. For example, NSGA-II was used to optimise three different TSA process configurations: (1) fixed-bed TSA with pellets, (2) fixed-bed TSA with hollow fibers, and (3) moving-bed TSA with pellets, by simultaneously minimising energy consumption and maximising productivity, resulting in Pareto fronts that satisfied the imposed constraints of 95 % CO_2 purity and 90 % recovery [29]. In another study by Bagheri et al. [30], NSGA-II was applied to optimise a TSA cycle design for ethane purification, aiming to minimise specific energy consumption while maximising hydrocarbon recovery and ethane productivity, resulting in valuable trade-off solutions.

For cyclic adsorption systems such as PSA and TSA, optimising performance indicators like purity, recovery, productivity, and specific energy consumption is essential, but computationally intensive [31]. This is due to the need for dynamic simulations to achieve cyclic steady-state conditions (CSS) under varying operational parameters, often requiring hundreds to thousands of CSS [32]. While steady-state approaches have reduced computational time for PSA/VSA processes [30], the TSA process remains challenging due to longer cycle durations in both dynamic and steady-state simulations [30]. In TVSA, the large number of operating variables increases and their strong interdependence with performance targets further complicate simulation and optimisation, making direct optimisation increasingly time and resource intensive. In our case, a single simulation run using the detailed process model takes up 2 to 10 min on a standard desktop computer, making multi-objective optimisation involving thousands of simulations practically infeasible. One approach to mitigate the high computational cost associated with detailed process simulations is the use of shortcut models [33,34], which simplify the underlying physics to reduce simulation time. Zhao et al. [35] employed a shortcut fixed-bed TSA model to compare various adsorbents and cycle configurations for post-combustion CO_2 capture. While this framework enabled rapid comparative assessment of the relation between cycle design and adsorbent properties, the authors suggesting that future studies should incorporate mass-transfer effects and bed configuration for more realistic evaluation. Such simplified models often omit critical descriptors from detailed

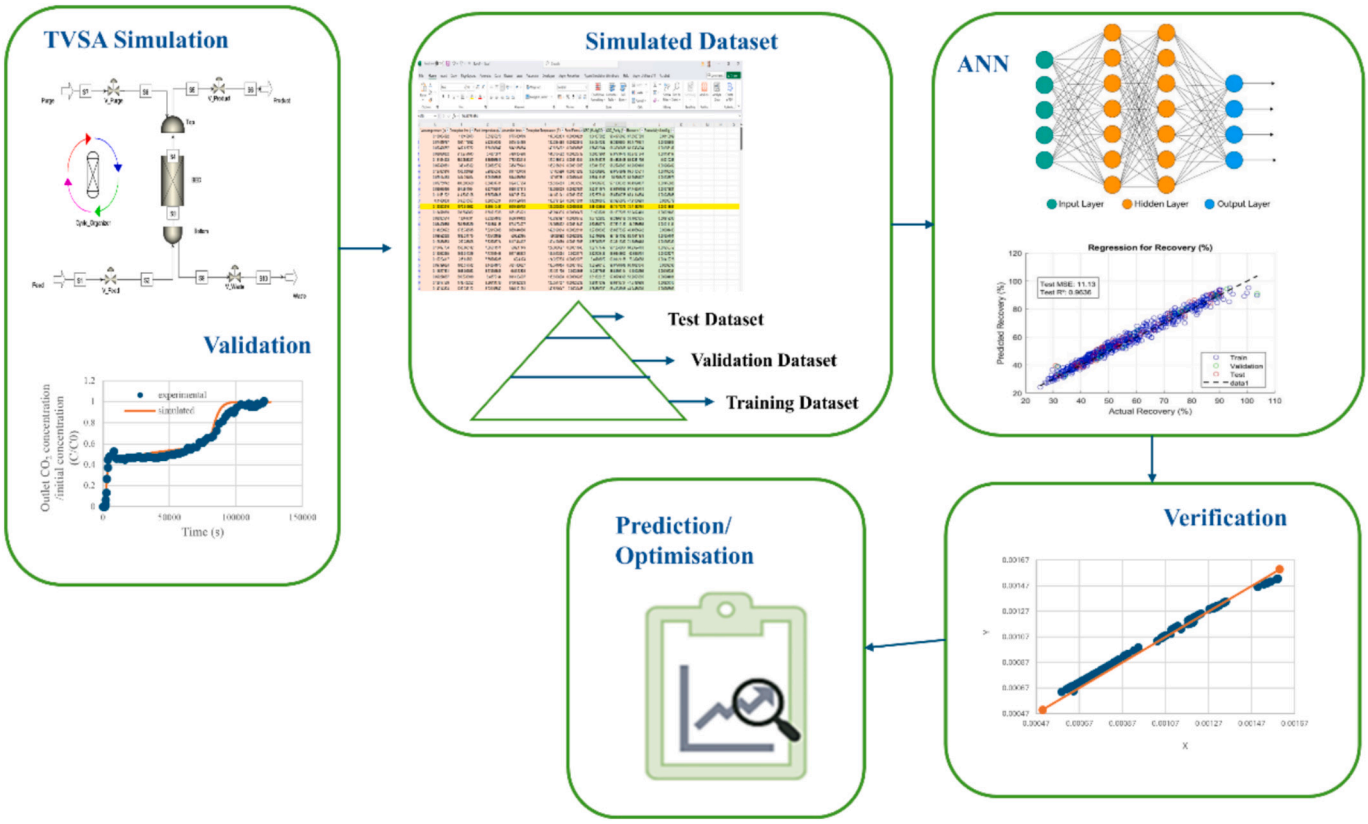

Fig. 1. Schematic of the optimisation procedures employed in this study.

Parameters	Units	Values
CO_2 heat of adsorption	KJ/mol	-71
N_2 heat of adsorption	KJ/mol	-18
Heat capacity of crystal	KJ/Kg. K	1.6
CO_2 Heat capacity	KJ/Kmol.K	37.4673
N_2 Heat capacity	KJ/Kmol.K	29.1806
Thermal conductivity	W/m.K	0.3

Parameters	Units	Values
Bed Length	m	0.055
Bed Internal Radius	m	0.004
Desorption Temperature	°C	115
Adsorption Temperature	°C	23
Particle Radius	m	2.25e-4
Crystal Density	Kg/m^3	860
Bed Porosity	-	0.32
Adsorbent Weight	g	60
Particle Porosity	-	0.85
Feed Flow rate	N ml/min	17.2

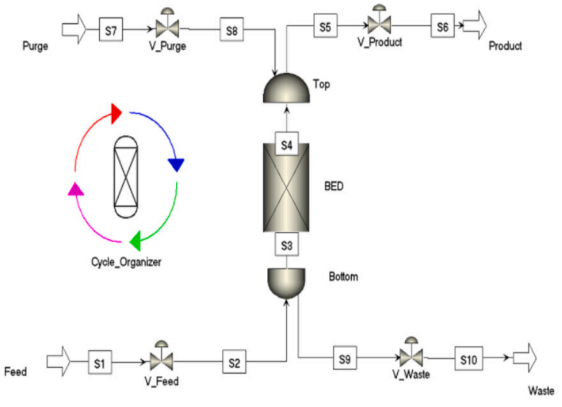

Cycles of Process	Duration (s)
Adsorption	7200
Evacuation	6
Heating + Evacuation	10000
Cooling	Event driven ($T_{Cooling} = T_{Feed}$)
Pressurising	Event driven ($P = P_{atm}$)

Fig. 2. Schematic of the TVSA process modelled in Aspen adsorption, along with a summary of input data and cycle organiser [43].

simulations, such as mass and heat transfer, which limits their applicability for systems involving slow adsorption kinetics, such as amine-functionalised sorbents [33,36].

An alternative and increasingly popular solution is the adoption of surrogate models, which aim to reduce problem dimensionality while maintaining the fidelity of the detailed simulations when trained on sufficiently large datasets [36]. Common Surrogate modelling techniques include support vector machine [37], radial basis function [38],

Table 1
Formulas for performance indicators.

Performance indicators	Unit	Formula
CO_2 purity	%	$\frac{\int_0^{t_{cycle}} F_{product} y_{CO_2} dt}{\sum_{i=1}^{m} \int_0^{t_{cycle}} F_{product} y_i dt}$
Recovery	%	$\frac{\int_0^{tcycle} \left(y_{product,CO_2} F_{product}\big\|_{z=L} \right) dt}{\int_0^{tcycle} \left(y_{feed,CO_2} F_{feed}\big\|_{z=0} \right) dt}$
Productivity	Kmol/kg.h	$\frac{3600 \times \int_0^{tcycle} \left(F_{product} y_{CO_2} \right) dt}{w_{adsorbent} t_{cycle}}$
SEC (vacuum)	MJ/kg CO_2	$\frac{\int_0^{t_{cycle}} \frac{F_{vac} P_{vac} \gamma}{\eta(\gamma - 1)} \left[\left(\frac{P_{feed}}{P_{vac}} \right)^{1-\frac{1}{\gamma}} - 1 \right] dt}{\int_0^{t_{cycle}} F_{product} y_{product,CO_2} dt}$

polynomial regression [39], artificial neural network (ANN) [40], and Gaussian process regression model [41]. With the broader rise of artificial intelligence (AI) in engineering applications, ANNs have found widespread use in CCS research, including simulating and optimising CO_2 capture processes, as well as for predicting effective physicochemical properties of sorbents. Du et al. [31] developed a hybrid surrogate-based framework integrating a convolutional neural network (CNN) with the NSGA-III algorithm to optimise a VPSA process for CO_2 removal from confined environments. Similarly, ANN-based surrogate models within an NSGA-II framework for PSA cycle optimisation have been employed by Subraveti et al. [42], for pre-combustion CO_2 capture. The results of these studies demonstrate that ANNs not only provide an accurate approximation of detailed capture processes, but also significantly reduce the computational time required for multi-objective optimisation.

This study developed a TVSA cycle incorporating both time- and event-driven steps to optimise the DAC process for a gas mixture containing N_2 and CO_2 at an atmospheric concentration of 400 ppm using mmen-Mg_2(dobpdc). A two-step approach was employed, coupling a neural network-based surrogate model with the NSGA-II algorithm for multi-objective optimisation. In the first step, an artificial neural network (ANN) with two hidden layers is trained on simulation data generated by the detailed TVSA model and verified using an independent dataset to predict key process indicators, including CO_2 purity, recovery, productivity, and Specific energy consumption (SEC). In the second step, NSGA-II is used to perform a multi-objective optimisation of the trained ANN surrogate model, with CO_2 recovery, productivity, and SEC defined as the objective functions. Finally, the process is analysed using performance indicators and decision variables, demonstrating how these variables influenced the process performance. The resulting Pareto solutions illustrate the trade-off between SEC and CO_2 recovery, providing valuable insights for DAC process design. Fig. 1 illustrates the complete workflow leading to the optimisation stage.

2. Process description and methodology

2.1. Modelling and simulation of TVSA process

A dynamic TVSA model was developed in Aspen Adsorption V14 to evaluate the technical performance of mmem-Mg_2(dobpdc) under DAC conditions. The software simulates the complete adsorption/desorption cycle by incorporating mass, energy, and momentum balances to predict system behaviour and evaluate key process performance indicators, including CO_2 purity, recovery, productivity, and SEC. A schematic of the TVSA process, the parameter values used in the simulation, and cycle durations are shown in Fig. 2. The feed gas mixture, containing 400 ppm CO_2 and 0.9996 % N_2, was introduced at 1.013 bar, 296.15 K, and a flow rate of 17.2 N mL/min. The governing equations and detailed modelling approach, including kinetic and equilibrium models and their parameters, are described comprehensively in our previous work [43]. The model is assumed to be one-dimensional, ignoring radial gradients, with constant adsorbent and wall properties. The gas mixture follows ideal gas behaviour. The partial differential equations (PDEs) are solved using the UDS1 discretisation method with 20 nodes. The adsorption process is non-isothermal and adiabatic, with heat conduction in both gas and solid phases, and local thermal equilibrium assumed (Ts = Tg). Heat of adsorption and heat capacities are considered constant. Pressure drop is calculated using the Ergun equation. CO_2 adsorption behaviour on mmen-Mg_2(dobpdc) is described by the Sips isotherm model. Adsorption kinetics is modelled using the linear driving force (LDF) approach below the step pressure and the Avrami fractional-order model above it [44]. The complete simulation methodology and results have been performed and reported in detail in [43], which is referenced here for modelling specifics.

2.2. Optimisation problem

The results from the structured sensitivity analysis [43] revealed that multiple process parameters significantly influence process performance, often through nonlinear interactions. A summary of these effects is presented below:

A decrease in feed temperature enhances the CO_2 adsorption capacity and prolongs the adsorption time. While this extended duration improves CO_2 recovery, it can negatively impact process productivity by reducing the number of annual cycles. To mitigate this drawback, increasing the feed flow rate offers an alternative approach, as it allows the system to reach saturation without significantly expanding the adsorption time. Reducing the vacuum pressure further contributes to improvement in CO_2 purity, recovery, and productivity by enhancing the thermodynamic driving force for desorption. However, this benefit comes at the cost of increased SEC. Notably, a relationship exists between feed temperature and the required vacuum pressure: lower feed temperatures shift the isotherm curve toward lower step pressures, allowing for more efficient desorption at milder vacuum conditions. In addition, the sorbent exhibits a threshold for heating temperature in the desorption step that is dependent on the applied vacuum level and desorption duration. At deeper vacuum pressures, the equilibrium partial pressure of CO_2 decreases, enabling effective desorption at lower temperatures [45], and it necessitates a prolonged desorption time. The duration of the desorption step also influences CO_2 purity and recovery, enhancing these metrics up to a specific limit. However, extended desorption times reduce productivity due to fewer operational cycles per year. Furthermore, there is a connection between desorption time and the thermal energy required for the desorption stage: longer desorption duration results in reduced heat demand for the regeneration step, which can positively affect SEC.

Due to the complex and interdependent effects of the process variables on process performance, the optimisation problem becomes highly intricate. Therefore, an advanced optimisation technique is necessary to identify optimal solutions by managing the trade-offs between selected performance indicators, TVSA operating parameters, and feed specifications. CO_2 Purity, recovery, productivity, and SEC are the key process performance indicators (PIs). The corresponding equations used to evaluate these indicators are presented in Table 1. The total energy demand consists of two components: electrical energy required by the vacuum pump and thermal energy supplied to the heat exchanger. The electrical energy consumption of the vacuum pump was calculated using the thermodynamic expression shown in Table 1, while thermal energy input for the heat exchanger was determined through Aspen Adsorption simulations. Due to the negligible pressure drop across the adsorption bed observed under experimental conditions, the energy consumption by the fan was considered insignificant and excluded from the overall energy analysis. In alignment with the requirements of DAC processes, the optimisation aims to maximise both recovery and productivity while minimising SEC. Six parameters influencing process performance were selected as decision variables, with their upper and lower bounds

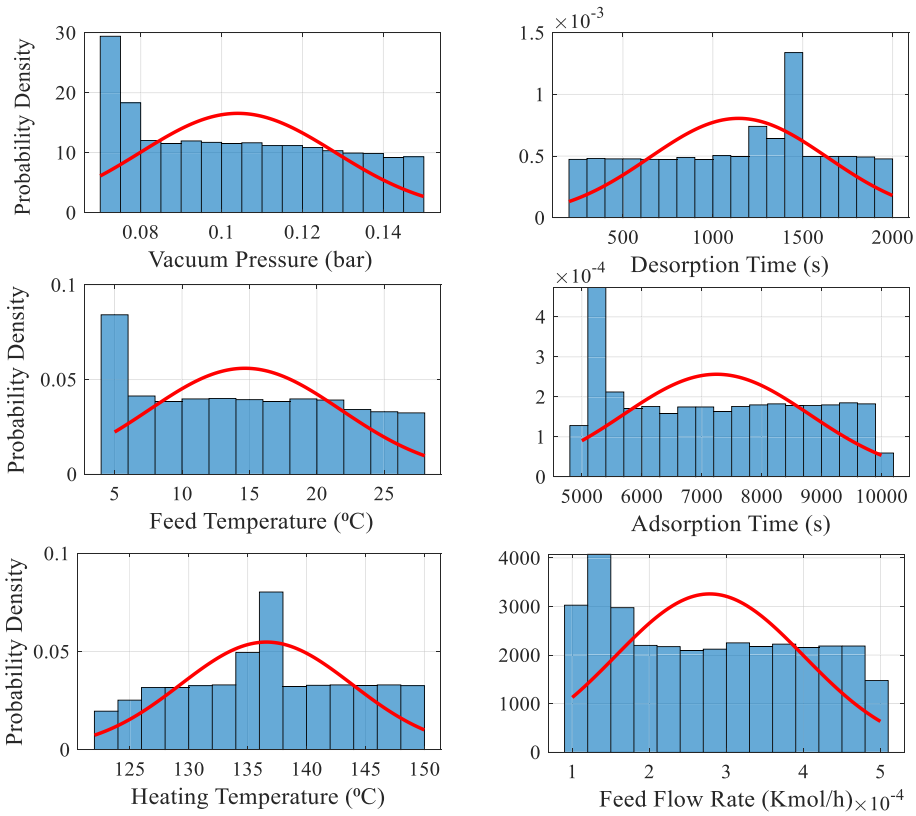

Fig. 3. The probability density distribution of each decision variable: vacuum pressure, desorption time, feed temperature, adsorption time, heating temperature, and feed flow rate, with overlaid normal probability density functions (red curves). (For interpretation of the references to colour in this figure legend, the reader is referred to the web version of this article.)

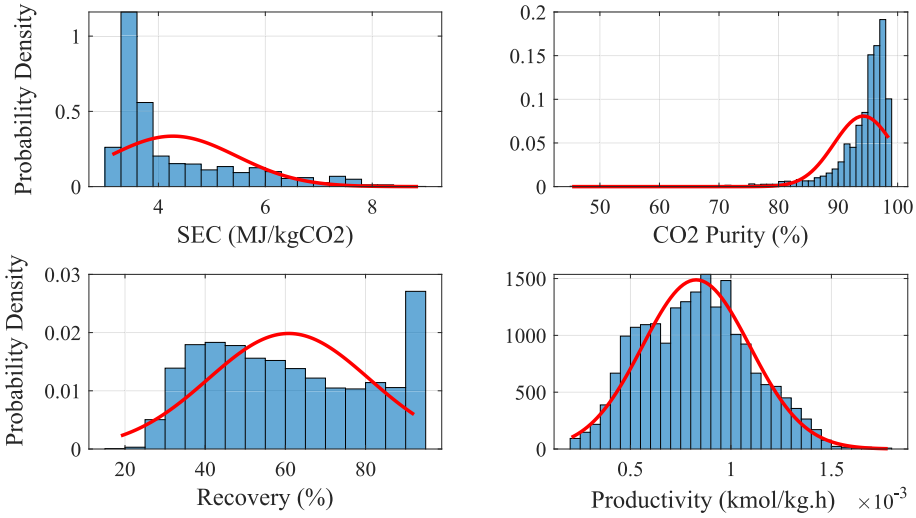

Fig. 4. The probability distributions of the performance indicators (SEC, CO_2 purity, recovery, and productivity), with overlaid normal probability density functions (red curves). (For interpretation of the references to colour in this figure legend, the reader is referred to the web version of this article.)

established through sensitivity analysis [43]. Constraining the decision variable ranges based on the sensitivity analysis results improved convergence and reduced the overall complexity of the optimisation problem.

2.3. Surrogate model development

2.3.1. Data generation and pre-processing

To develop the data-driven component of the surrogate model using various neural network algorithms, it was essential to generate a broad, uniform, and sufficiently large dataset. The comprehensiveness and diversity of the training data significantly influence the accuracy, robustness, and predictive capability of the surrogate model results. To ensure both adequate randomness and full coverage of the design space, the Latin Hypercube Sampling (LHS) method was employed for data generation [46]. A MATLAB-based interface was developed to automate the transfer of generated design points to Aspen Adsorption and to extract simulation output data into Microsoft Excel. A total of 2500

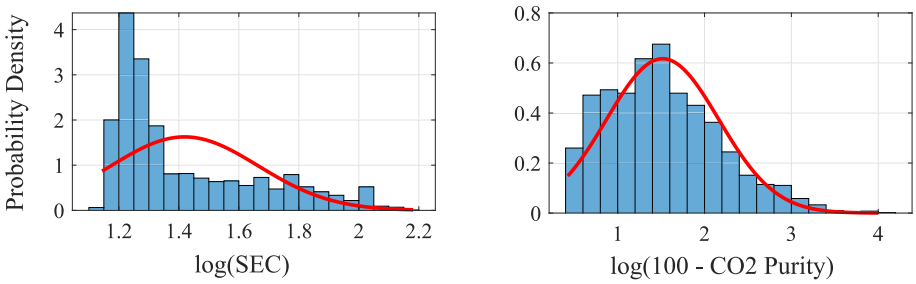

Fig. 5. The probability density distribution of SEC, and CO_2 purity after log transformation, with overlaid normal probability density functions (red curves). (For interpretation of the references to colour in this figure legend, the reader is referred to the web version of this article.)

samples were generated using the LHS approach, covering a wide range of operational conditions defined by the selected decision variables. The generated operating conditions were simulated using Aspen Adsorption under the TVSA model, and performance indicators – CO_2 purity, recovery, SEC, and productivity- were extracted from the simulation result. To ensure the accuracy of the dataset, the Aspen adsorption model was first validated against experimental data [43].

Fig. 3 presents the frequency distribution of each decision variable and normal probability density functions. The decision variables follow a uniform distribution, reflecting the use of LHS sampling. In contrast, the frequency distribution of performance indicators shown in Fig. 4 does not exhibit a normal distribution. Notably, CO_2 purity shows a right-skewed distribution, while SEC displays a pronounced left tail, indicating a wide range of simulation outcomes for these metrics. The observed skewness originates from the intrinsic behaviour of the Aspen Adsorption model rather than the sampling method. The input variable ranges were defined through preliminary single-variable sensitivity analyses to exclude unrealistic operating conditions. Thus, the skewed distributions reflect genuine process responses within the feasible DAC design space. In the subsequent stage of data pre-processing, a logarithmic transformation is applied to CO_2 purity and SEC, shown in Fig. 5, to address their pronounced skewness. This transformation helps approximate a normal distribution and improve the data symmetry of these performance indicators. Additionally, due to the substantial differences in the order of magnitude between the individual input and output variables, data normalisation is required before model training. A normalisation is performed using the functions described in Eqs. 1 and 2, where x and y represent the original input and output values, respectively; normalised denotes the scaled value; min and max correspond to the minimum and maximum values of each feature. Finally, the entire dataset is divided into a training, validation, and test sets with a ratio 80 %:10 %:10 %.

$$x_{normalised} = \frac{x_i - x_{min}}{x_{max} - x_{min}} \quad (1)$$

$$y_{normalised} = \frac{y_i - y_{min}}{y_{max} - y_{min}} \quad (2)$$

2.3.2. Surrogate model structure and training

An ANN model comprises three types of layers: an input layer, one or more hidden layers, and an output layer, all composed of interconnected processing units known as neurons. The input features of the ANN model include feed flow rate, feed temperature, vacuum pressure, adsorption time, desorption time, and the heat requirement for regeneration parameters, which are recognise for their significant impact on process performance. The outputs of the ANN model are CO_2 purity, recovery, SEC, and productivity, which are considered reliable performance indicators for evaluating the system.

In the development of data-driven models like ANN, determining the appropriate hyperparameters – including the number of hidden layers, the number of neurons in each layer, the activation functions, and the training algorithm are crucial for model accuracy and generalisation. In this study, the heuristic approach of manual trial and error was initially used to assess the suitability of different activation functions. However, to more systematically and efficiently determine the full network architecture, we adapted a genetic algorithm (GA) as a hyperparameter optimisation strategy. GAs are population-based metaheuristic search methods inspired by the principles of natural selection and genetics. They operate by evolving a population of candidate solutions (ANN configurations) through processes such as selection, crossover, and mutation, iteratively searching for architectures that maximise model performance. There are some studies that use the GA approach for selecting the surrogate model structure [47,48].

Three critical aspects of the ANN design are optimised through the GA algorithm: (1) the number of hidden layers (up to three), as increasing network depth on small datasets makes them prone to generating overfitted models, reducing generalisation ability [49], while too few layers may result in underfitting, limiting the network capacity to capture complex patterns [50]. This issue is particularly pronounced in models with high complexity and high-dimensional training patterns, where the model performance can significantly degrade on unseen data. (2) The number of neurons in each hidden layer, which influences the network's ability to capture the nonlinear relationship between inputs and outputs. Too many neurons may lead to overfitting, while too few may cause underfitting. (3) The type of activation function used in hidden layers, which affects the network's learning dynamics and approximation capability. Each candidate ANN generated within the GA population was constructed with different architectural parameters (e.g., number of layers activation function). Each network was trained on the predefined training dataset, and its performance was then evaluated using a separate validation dataset. This procedure allowed the GA to assess networks based on their validation accuracy and progressively evolve toward architectures with improved predictive performance. The coefficient of determination (R^2), the root mean square error (RMSE), and average absolute relative deviation (AARD) were used as evaluation metrics to assess the predictive accuracy and reliability of different neural network architectures. R^2 evaluate how well the predicted values match the actual data, AARD measures the average absolute relative error between actual and predicted values, and RMSE quantifies the average magnitude of prediction error. These metrics are calculated using the formulas 3 to 5, Where y_{actual} is the actual target value obtained by simulation, $y_{predicted}$ is the predicted value from the ANN, $y_{actual,ave}$ is the mean of the actual target values, i is the index of data samples, and n is the number of data points. Following the initial optimisation of the ANN architecture using the GA, the best-performing network configuration, identified based on the evaluation metrics, R^2, RMSE, and AARD, is selected for further validation. To assess the generalisability and reliability of the surrogate model, the selected ANN was integrated into the NSGA-II framework. NSGA-II was executed multiple times using the GA-derived ANN to generate a diverse set of pareto solutions. Each design proposed by the ANN was then input into Aspen Adsorption to compute the key performance indicators; CO_2 purity, recovery, productivity, and SEC. Subsequently, the performance metrics predicted by the ANN were independently validated by comparing them against the

Table 2
Range of Decision variables used in the optimisation process.

Process parameters	Unit	Lower bond	Upper bond
Adsorption time	s	5000	10,000
Desorption time	s	200	2000
Vacuum pressure	Bar	0.07	0.15
Heating temperature	^{0}C	120	150
Feed flow rate	Kmol/h	1 e-4	5 e-4
Feed temperature	^{0}C	5	30

corresponding values obtained from Aspen simulations. This comparison enabled a comprehensive assessment of the surrogate model's predictive accuracy in representing the true process behaviour across a wide range of operating conditions. The procedures for developing the ANN are shown in Fig. 6.

$$R^2 = 1 - \frac{\sum_{i=1}^{n}\left(y_{actual} - y_{predicted}\right)^2}{\sum_{i=1}^{n}\left(y_{actual} - y_{actual,ave}\right)^2} \tag{3}$$

$$RMSE = \sqrt{\frac{1}{n}\sum_{i=1}^{n}\left(y_{actual} - y_{predicted}\right)^2} \tag{4}$$

$$AARD = \frac{100}{n}\sum_{i=1}^{n} abs\left(\frac{y_{actual} - y_{predicted}}{y_{actual}}\right) \tag{5}$$

2.4. TVSA process optimisation

After developing the surrogate model, determining the optimal parameter configuration, and rigorously validating its predictive accuracy, the NSGA-II algorithm was employed to perform multi-objective optimisation of the TVSA process, targeting three conflicting objectives: productivity, recovery, and SEC. NSGA-II was selected due to its ability to overcome shortcomings of traditional evolutionary algorithms, such as the lack of elitism and the reliance on manually defined sharing parameters [28]. A key strength of multi-objective optimisers like NSGA-II lies in their capacity to generate a well-distributed Pareto front, enabling informed decision-making by revealing the trade-offs among competing objectives [51]. The NSGA-II algorithm is often employed as a benchmark for evaluating the performance of new optimisation algorithms [28]. In this study, NSGA-II is integrated with an ANN to optimise key performance metrics of the process, including CO_2 purity, recovery, productivity, and SEC. The selected decision variables are adsorption time, desorption time, vacuum pressure, heating temperature, feed flow rate, and feed temperature. The flow chart illustrating the procedures of the NSGA-II algorithm is shown in Fig. 7. The optimisation process

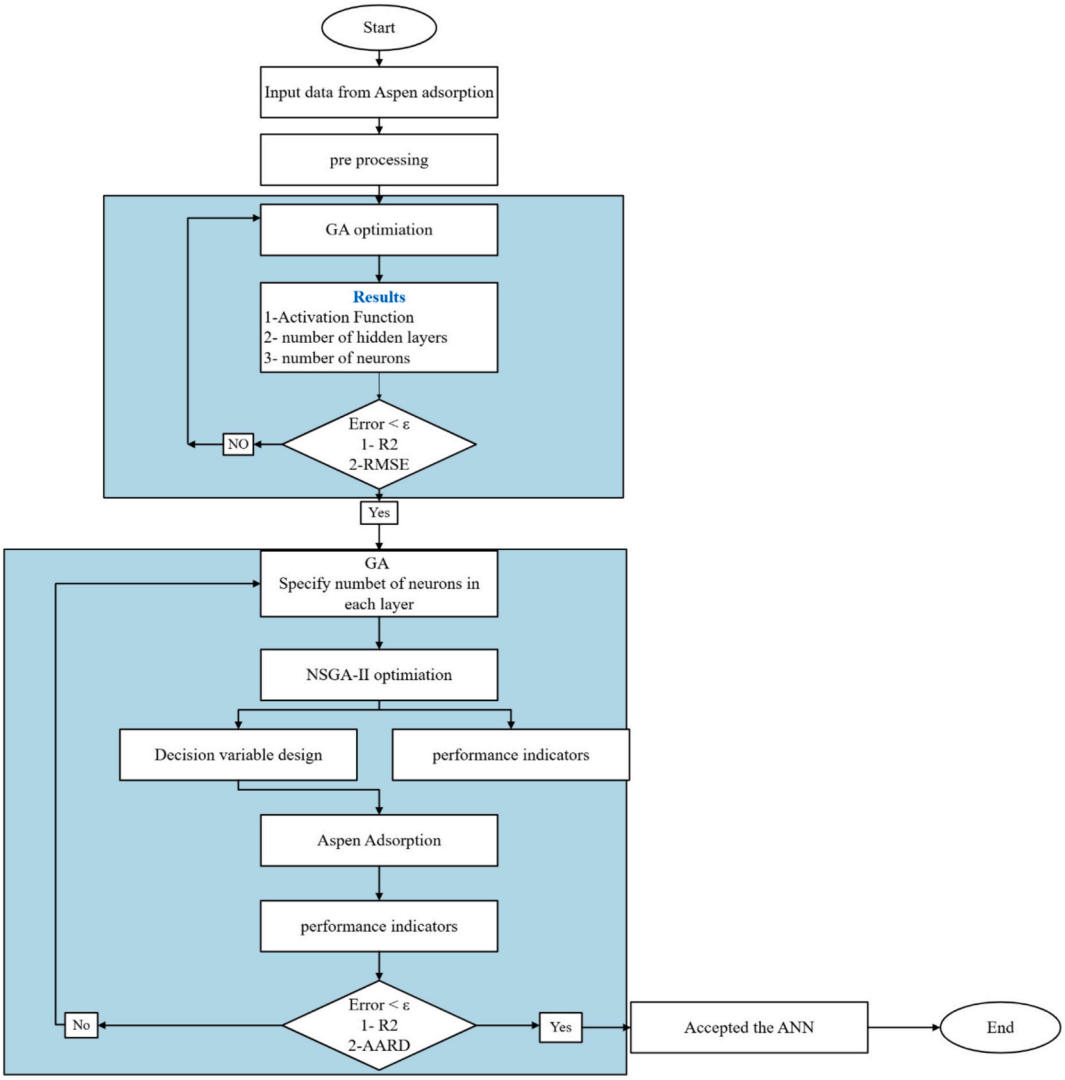

Fig. 6. Flowchart of the procedure for developing the ANN model, from data generation to final model construction.

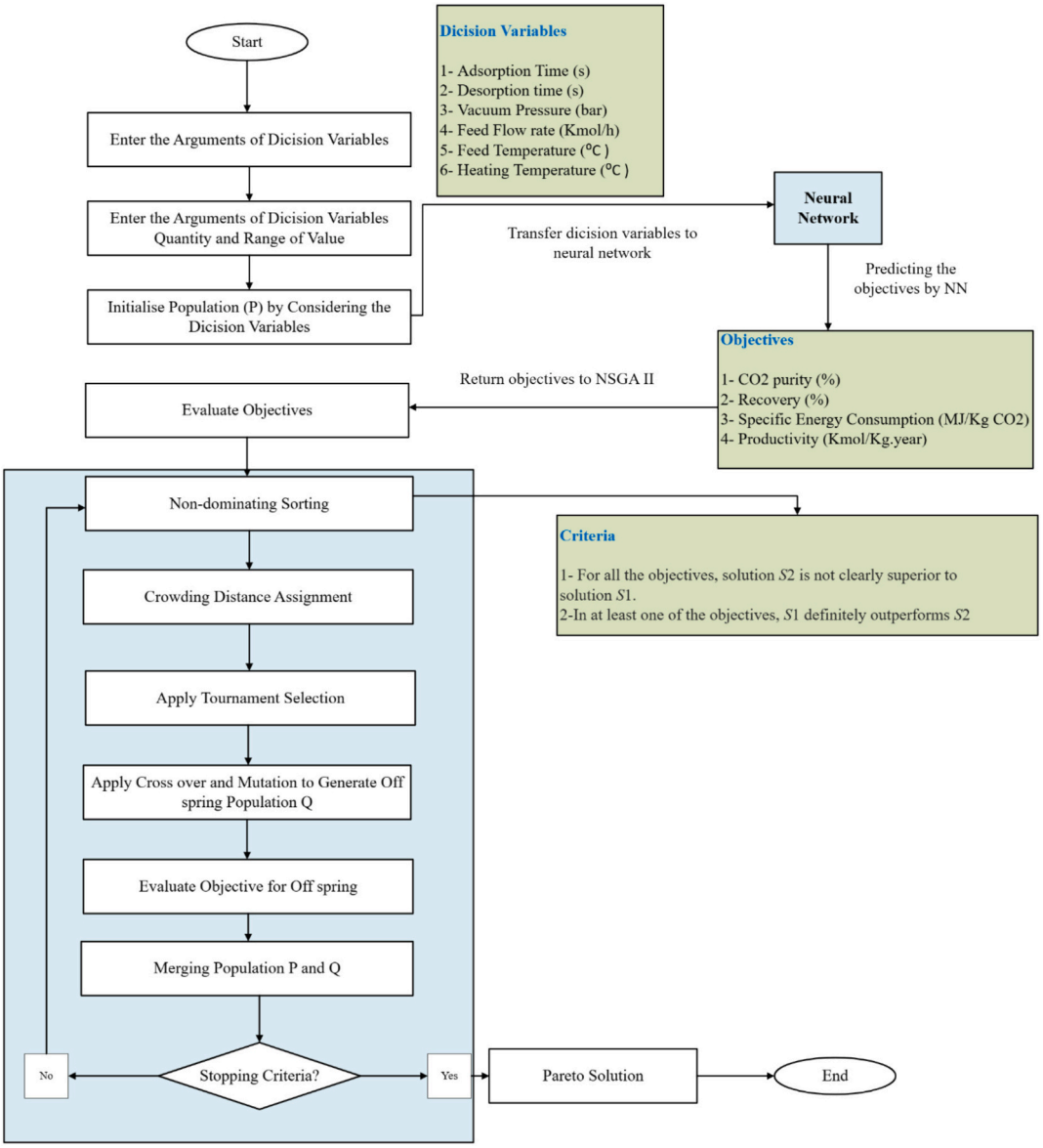

Fig. 7. Flowchart of the sequence of procedure in the NSGA-II optimiser.

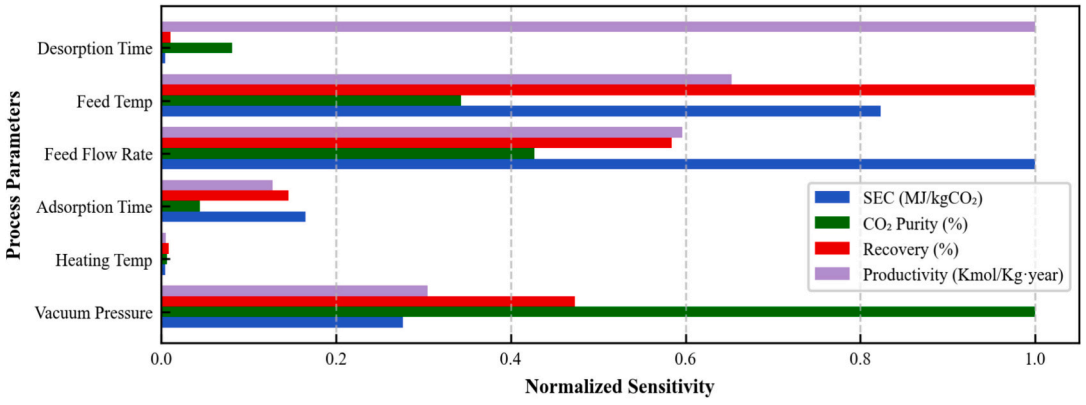

Fig. 8. The results of sensitivity analysis of six decision variables on the CO_2 purity, recovery, specific energy consumption and productivity [44].

begins with the initialisation of a population within NSGA-II, where each encodes are potential solutions defined by a specific set of decision variable values. These values are transferred into the trained ANN model, which estimates the corresponding performance metrics-CO_2 purity, recovery, productivity, and SEC. The predicted outcomes are then fed back to the NSGA-II algorithm for fitness evaluation. NSGA-II

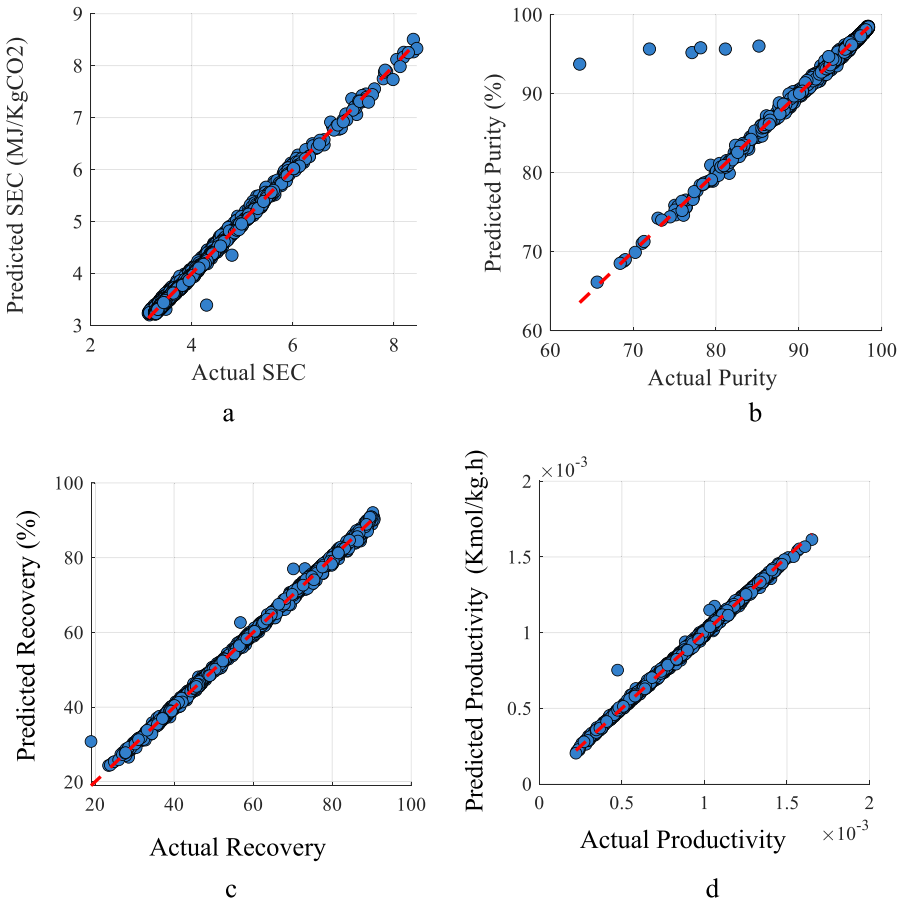

Fig. 10. Comparison the training dataset for actual values (from software) and predicted values (from ANN model) of four process performance indicators, where (a) represents the SEC, (b) shows the CO_2 purity, (c) displays the recovery, and (d) shows the productivity.

ranks the population using a non-dominated sorting approach, classifying individuals into different Pareto fronts. The first front consists of non-dominated solutions, while subsequent fronts are incrementally dominated by those preceding them. To maintain solution diversity, a crowding distance is calculated for each individual within the same front, quantifying its proximity to neighbouring solutions. Selection of solutions is performed using a binary tournament, considering both their rank and crowding distance. Solutions with a higher rank are selected first. When solutions share the same rank, preference is given to the one with the greater crowding distance. The selected individuals undergo crossover and mutation to generate a new offspring population. This new offspring is then combined with the parent population, and the combined pool is re-sorted using non-dominated sorting. The top-performing solutions based on rank and crowding distance are carried forward to the next generation. This iterative process continues until a specific number of generations is reached. The final output is a set of Pareto-optimal solutions, offering trade-offs among the conflicting objectives. The selection of an appropriate population size and the maximum number of generations in an optimisation problem typically depends on the complexity of the process and is often refined through trial and error to achieve the desired level of accuracy.

3. Results and discussion

3.1. Process simulation

The TVSA process model was previously developed and validated against experimental data. Following this, an extensive sensitivity analysis was conducted to evaluate the influence of key operational parameters on process performance. The full details of this analysis, including the impact of each parameter and the corresponding graphical results, are presented in [43]. Fig. 8 presents the results of the sensitivity analysis, highlighting the influence of each selected parameter on the key performance indicators. These parameters were prioritised based on their significant impact on performance indicators such as CO_2 purity, recovery, productivity, and SEC. Based on the outcomes of the sensitivity study, a set of decision variables and their corresponding ranges were identified, as summarised in Table 2. These ranges are consistently used to generate a simulation dataset of 2500 samples for neural network training using the LHS approach and also served as input bounds for the NSGA-II optimisation framework. This structured methodology ensures that both the surrogate model and optimisation process are grounded in realistic and physically meaningful operating conditions.

3.2. ANN-surrogate model: Development and reliability analysis

The ANN model is trained using 2500 data samples generated from the Aspen Adsorption simulations. The structure of the surrogate model and its optimal hyperparameters have been determined through a systematic multi-step procedure, as illustrated in Fig. 6. (See Fig. 9.) (See Fig. 16.)

After separating the dataset into training, validation, and test (80 %, 10 %, and 10 % respectively), in the first step, the number of hidden layers and the type of activation function are specified using a GA algorithm optimisation framework. Over 1000 neural network configurations are evaluated, varying in the number of hidden layers (ranging from 1 to 3), the number of neurons per layer, and the activation function (either logsig or tansig). Each configuration was assessed based on its performance on both training and validating datasets, using the R^2

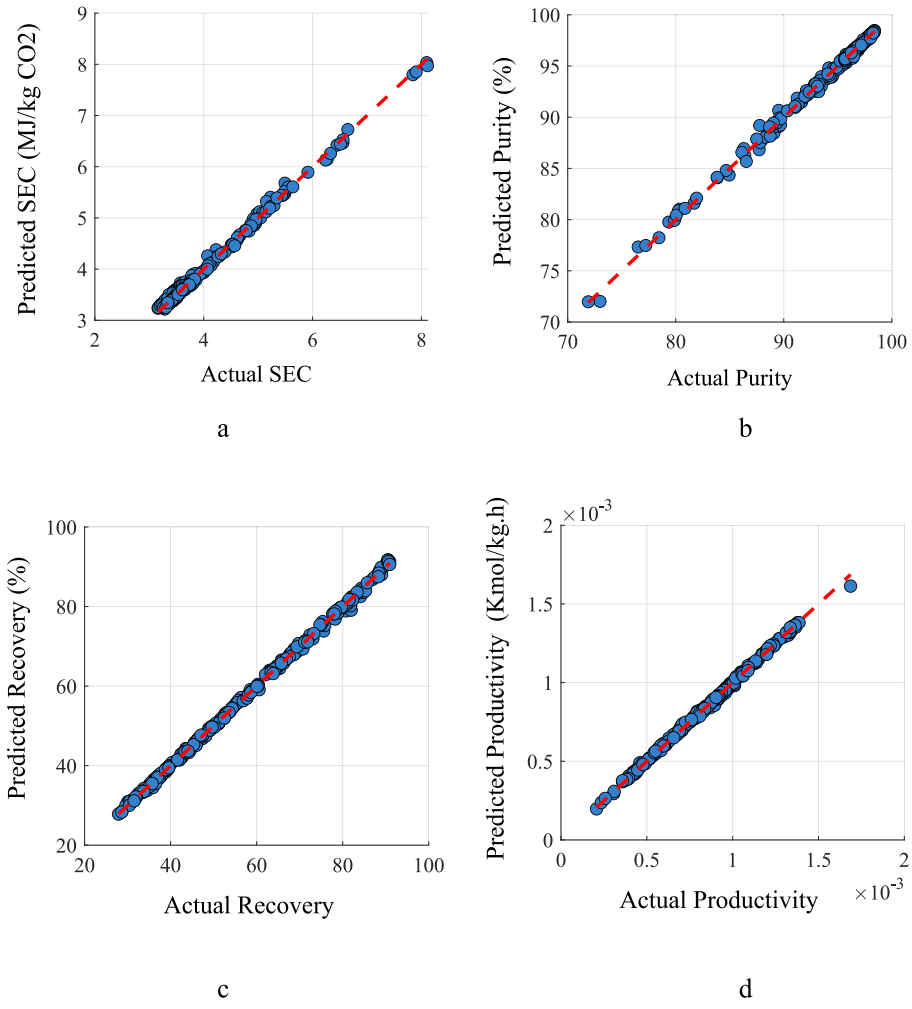

Fig. 11. Comparison the validation dataset for actual values (from software) and predicted values (from ANN model) of four process performance indicators, where (a) represents the SEC, (b) shows the CO_2 purity, (c) displays the recovery, and (d) shows the productivity.

and RMSE as performance metrics. The comparison results are summarised in Fig. 9a, and b for different hidden layer counts and Fig. 9c and d for different activation functions. As shown, the architecture with two hidden layers exhibited the best overall performance, achieving the highest R^2 and lowest RMSE values. Similarly, the logsig activation function (represented as option 2 in Fig. 9c and d) outperformed tansig (represented as option 1 in Fig. 9c and d) in terms of predictive accuracy. Based on these findings, a two-hidden-layer architecture with logsig as the activation function is selected.

Following determining the optimal optimiser and activation function, the next step involves selecting the appropriate number of neurons in each hidden layer. The GA provides an initial estimate for the number of neurons, which is used as a baseline. With the constant activation function and number of hidden layers, the GA returns to optimise the number of neurons in each layer. The resulting network configurations are trained, and their performance is evaluated based on both the validation and testing datasets. After each iteration, the ANN model undergoes further validation to assess and refine its predictive accuracy. The outputs of the ANN model are compared with simulation results from Aspen Adsorption for a new set of input decision variables. The number of neurons was iteratively refined through successive GA runs until a satisfactory agreement was achieved between the neural network predictions and the simulator outputs. This final comparison served to verify the surrogate model's capability to accurately replicate the simulation behaviour. The final network architecture consists of 17 neurons in the first hidden layer and 8 neurons in the second hidden layer. The performance of the ANN model during training and validation phases is shown in Fig. 10 and Fig. 11, respectively. The accuracy of the ANN model is evaluated by comparing its prediction with the actual dataset from Aspen Adsorption in the test dataset, displayed in Fig. 12. Furthermore, the corresponding R^2 values, AARD and RMSE metrics for the training, validating, and testing datasets are reported Table 3. As shown, the selected ANN model is characterised by high predictive accuracy, with the highest R^2 values and the lowest RMSE and MAPE on the testing dataset, indicating robust generalisation and reliable predictive performance for the DAC process investigated in this study. The performance of the final surrogate model in comparison with the Aspen adsorption outputs for a new dataset is also illustrated in Fig. 13. Table 4 summarises the R^2 and AARD results, demonstrating high accuracy of the model in predicting the process outputs. Therefore, the selected ANN architecture comprised two hidden layers with an optimised number of neurons in each. The logistic sigmoid (logsig) was used in the hidden layers, while the linear activation function (purelin) was applied in the output layer. Network training was performed using the Bayesian regularisation backpropagation algorithm (trainbr). Training was conducted for a maximum of 1000 epochs, with convergence monitored through a gradient threshold of 1e-9. To enhance robustness and avoid overfitting, early stopping was implemented through a maximum validation failure tolerance of 9 consecutive epochs. The training is executed without the graphical training window to ensure reproducibility and streamline execution. (See Table 4.)

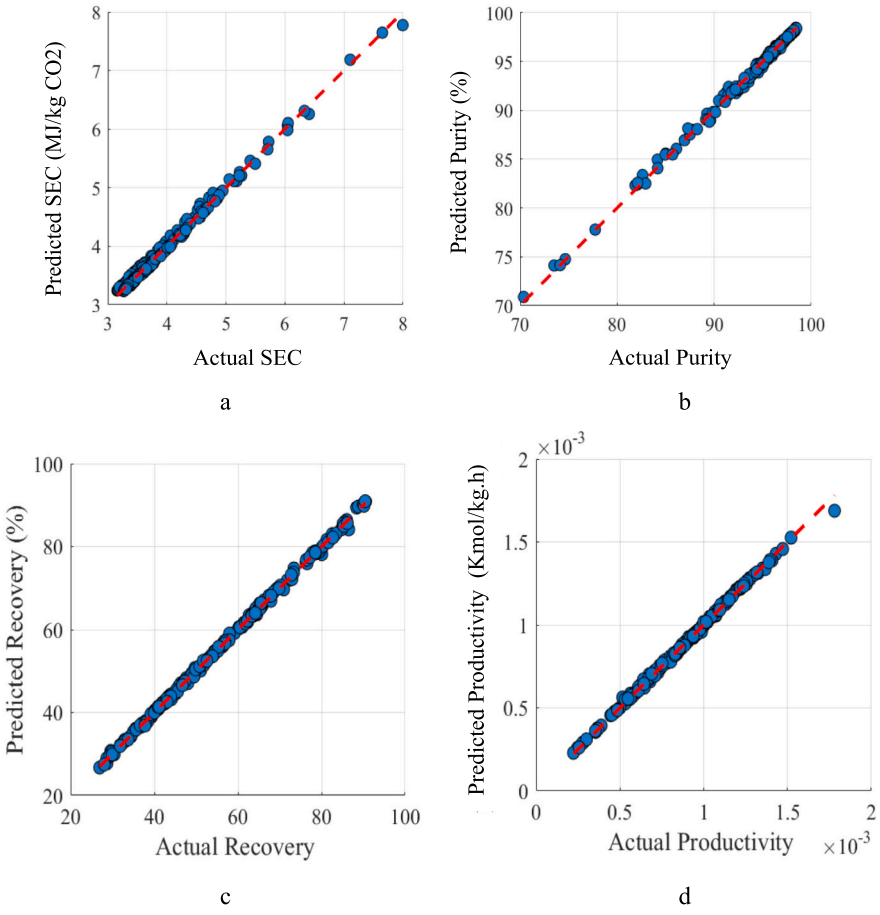

Fig. 12. Comparison the test dataset for actual values (from software) and predicted values (from ANN model) of four process performance indicators, where (a) represents the SEC, (b) shows the CO_2 purity, (c) displays the recovery, and (d) shows the productivity.

3.3. Multi-objective process optimisation by surrogate model

Once the validity of the ANN model was confirmed, the NSGA-II algorithm was integrated with the ANN model to perform the multi-objective optimisation of the TVSA process. The parameters of the NSGA-II were empirically calibrated through multiple computational trial-and-error procedures, with the final values present in Table 5. The crossover and mutation probabilities are set to 0.9 and 0.1, respectively, and a standard value of 20 is applied to both the crossover and mutation indices. Fig. 14 shows the progression of the best solution across generations for each objective function: recovery, productivity, and SEC. Since recovery and productivity are maximised, while SEC is minimised, the normalised fitness values converge toward 1 and 0, respectively. The optimisation process stabilises around generation 850, where the best fitness value reaches their optimal levels. Based on this behaviour, the population size and number of generations are fixed at 250 and 1000, respectively.

The outcomes of the optimisation process are represented as a Pareto front, which consists of non-dominated solutions. In other words, none of these solutions is universally superior; rather, each reflects trade-offs and demonstrates advantages in at least one objective compared to others. The Pareto front may contain an infinite number of mathematically incomparable solutions, each reflecting a unique balance among competing objectives. Every point on the Pareto front corresponds to a specific combination of decision variables that can be considered as a viable design strategy [52]. Consequently, the optimisation provides a diverse set of optimal configurations for potential implementation. The 3D Pareto front for CO_2 recovery, productivity, and SEC is shown in Fig. 15, with CO_2 purity indicated by colour. Designs indicated in blue, which exhibit low purity and recovery, are excluded from further analysis in this study. The remaining designs achieve CO_2 purity above 94 %, which is considered the target threshold for this work. As observed in this figure, increases in productivity and recovery are accompanied by higher SEC, but two distinct trends can be observed. To explore this relationship further, 2D Pareto fronts of recovery versus productivity are presented in **Error! Reference source not found.** The data points form two distinct clusters. In both clusters, a clear direct relationship is seen between productivity and recovery. However, cluster two exhibits higher SEC for similar recovery levels compared to cluster 1 (dark blue point), reflecting the trade-off between improved productivity and greater energy consumption. Additionally, following the yellow and green data points - representing designs with high SEC and high productivity, respectively - it becomes clear that, although both sets achieve strong performance, they differ in terms of recovery and productivity. The yellow designs, which consume more energy, attain the highest CO_2 recovery, albeit with slightly lower productivity compared to the green group. In contrast, the green designs require more energy and achieve slightly lower recovery (around 84–87 %), but they offer the highest productivity among all configurations. This highlights the inherent trade-offs and emphasises the need to balance process performance and energy requirements carefully.

Building on the findings from the sensitivity analysis, several key trends were identified regarding the impact of individual decision variables on process performance which are summarised in section 2.2.

However, unlike sensitivity analysis- which evaluates the effect of one variable at a time- the optimisation process considers the combined influence of all decision variables simultaneously. This enables the optimiser to explore the full design space and identify design

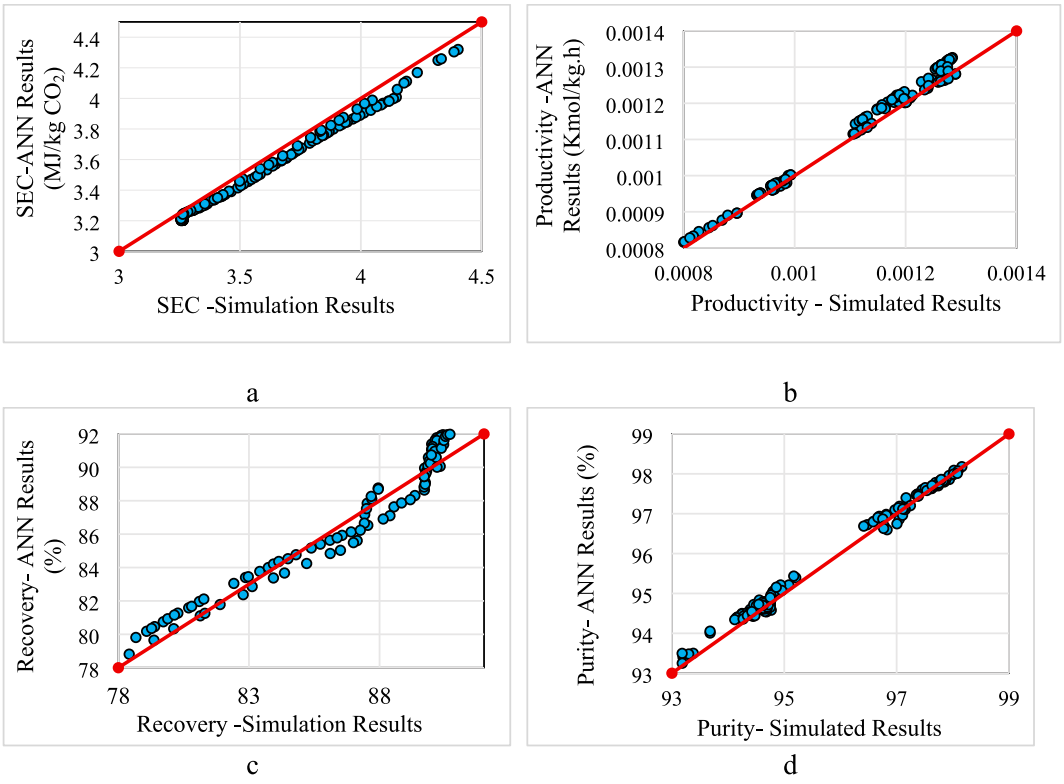

Fig. 13. Final testing results of the ANN using a new dataset evaluated through the simulator, where (a) represents the SEC, (b) shows productivity, (c) displays recovery, and (d) represents CO_2 purity.

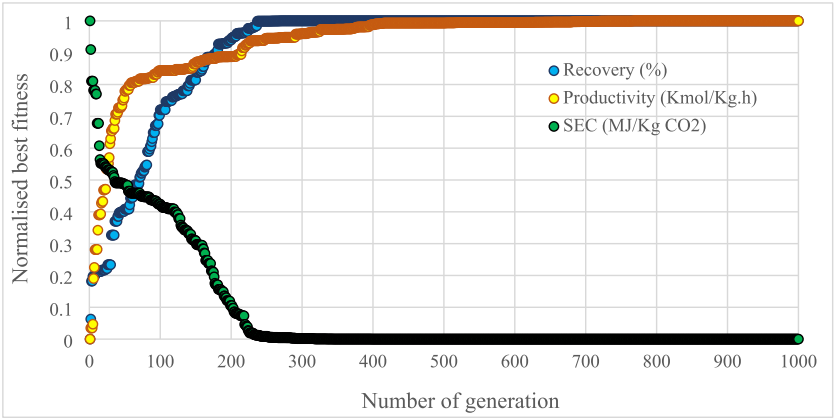

Fig. 14. Number of generation required for convergence with a constant population of 250. The NSGA-II model was terminated upon stabilisation of values across the three objective functions: SEC, productivity, and recovery.

configurations that achieve the best overall balance between productivity, recovery, and SEC, considering the interdependent and nonlinear effects revealed by the sensitivity analysis. To further understand the role of each decision variable in shaping these outcomes, an exploration range analysis was conducted. The spread of each variable along the x-axis in these figures reflects its influence on the productivity and SEC (Fig. 17) and recovery and SEC (Fig. 18). Based on this analysis, feed flow rate, adsorption time, and vacuum pressure emerged as the most influential decision variables. The feed flow rate is varied from 1e-4 to 4e-4 Kmol/h - an increase of 300 % - highlighting its significant influence on system performance. As the feed flow rate increases up to 3e-4 Kmol/h, productivity rises steadily from approximately 0.8 to 1.68 Kmol/kg.h, more than doubling. This trend is accompanied by the modest increase in both recovery and SEC, with SEC rising from 3.2 to 3.8 MJ/kg CO_2, and recovery increasing from 75 % to 95 %. However, further increasing the flow rate from 3e-4 to 4e-4 Kmol/h results in a slight improvement in productivity (from 1.68 to 1.78 e-3 Kmol/kg.h) along with a reduction in SEC (from 3.6 to 3.2 MJ/kg CO_2), but at the expense of reduced recovery (falling from 88 to 78 %). This trade-off highlights the delicate balance between productivity, SEC, and recovery when optimising the feed flow rate.

Additionally, the adsorption time is varied from 5000 to 10,000 s, representing a 100 % change. The substantial variation, along with the wide range in feed flow rate, indicates that both parameters were thoroughly explored during the optimisation process and are critical to achieving optimal performance. Given their strong individual and combined impact, their interaction is illustrated in Fig. 19, where adsorption time is plotted on the x-axis and feed flow rate on the y-axis,

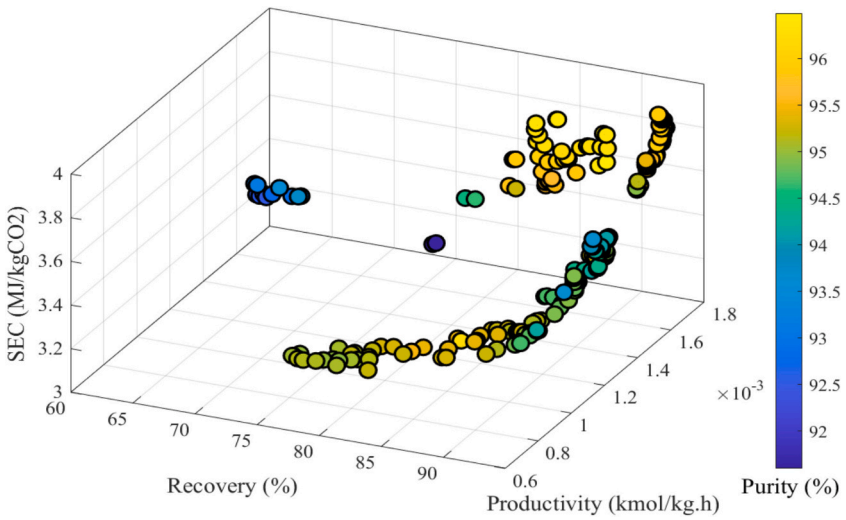

Fig. 15. Three-dimensional Pareto front illustrating the trade-offs among SEC, productivity, and recovery.

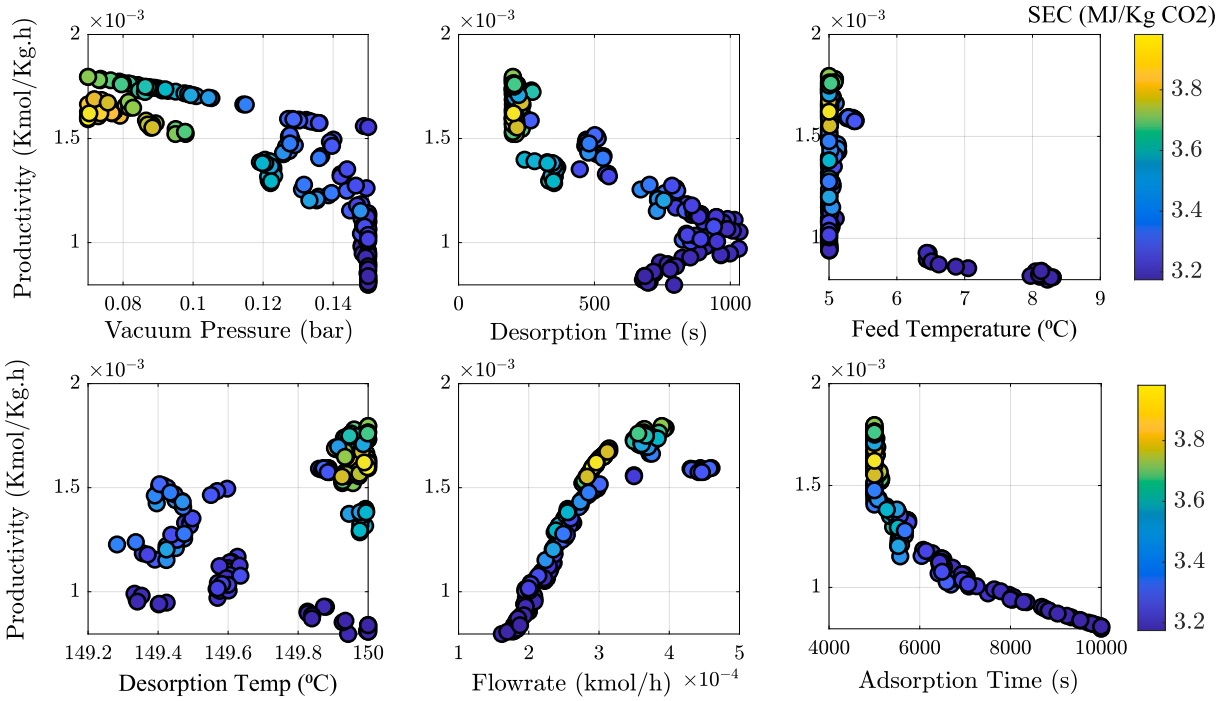

Fig. 17. Effect of operational parameters on the Pareto front with productivity and SEC represented by colour.

with productivity, purity, recovery, and SEC represented by colour gradients in each subplot. The results reveal an inverse relationship between these two parameters in the search for optimal designs: as adsorption time increases, achieving optimal performance requires a reduction in feed flow rate. This reflects the need to allow sufficient time for bed saturation and effective CO_2 uptake, depending on the rate of CO_2 supply. Regarding vacuum pressure, which varies from 0.07 to 0.15 % bar(a 114 % change), Fig. 17 and Fig. 18 show that increasing vacuum pressure generally leads to reduced productivity and recovery. However, this comes with the benefit of improved energy efficiency, as SEC is significantly lowered. Previous studies have indicated that a vacuum pressure of 0.15 bar generally fails to achieve high levels of productivity and recovery (reference). In this study, the optimisation results support this observation: at a vacuum pressure of 0.15 bar, the maximum achievable recovery (94 %) and productivity (1.8 e-3 Kmol/kg.h) were not achieved. However, several designs operating at this pressure still demonstrated reasonably high performance while benefiting from reduced energy consumption. This implies that the limitations of higher vacuum pressures can be offset by appropriately adjusting other decision variables. For instance, at a fixed vacuum pressure of 0.15 bar, recovery and productivity varied between 73 and 92 % and 0.8–1.6 e-3 Kmol/kg. h, respectively, depending on the combination of other parameters. Notably, the energy consumption across all these configurations remained around 3.2 MJ/kg CO_2, which is substantially lower than the maximum observed value of 3.9 MJ/kg CO_2. This highlights the potential of synergistic parameter tuning to mitigate energy demands while maintaining acceptable process performance.

In contrast, the heating temperature showed minimal variation during optimisation, ranging from 149 to 150 °C, a change of lower than 1 %. As observed in the sensitivity analysis, temperatures below 120 °C were insufficient for effective CO_2 desorption, indicating that a minimum threshold temperature is required for this sorbent to function

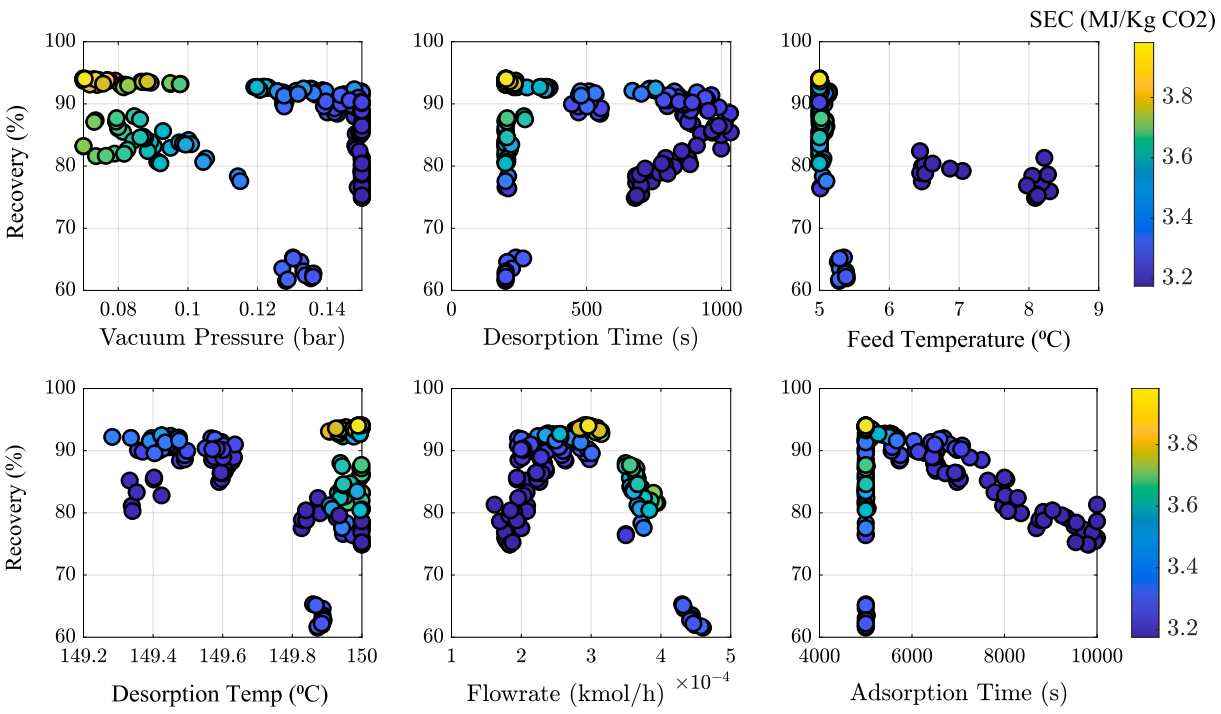

Fig. 18. Effect of operational parameters on the Pareto front with recovery and SEC represented by colour.

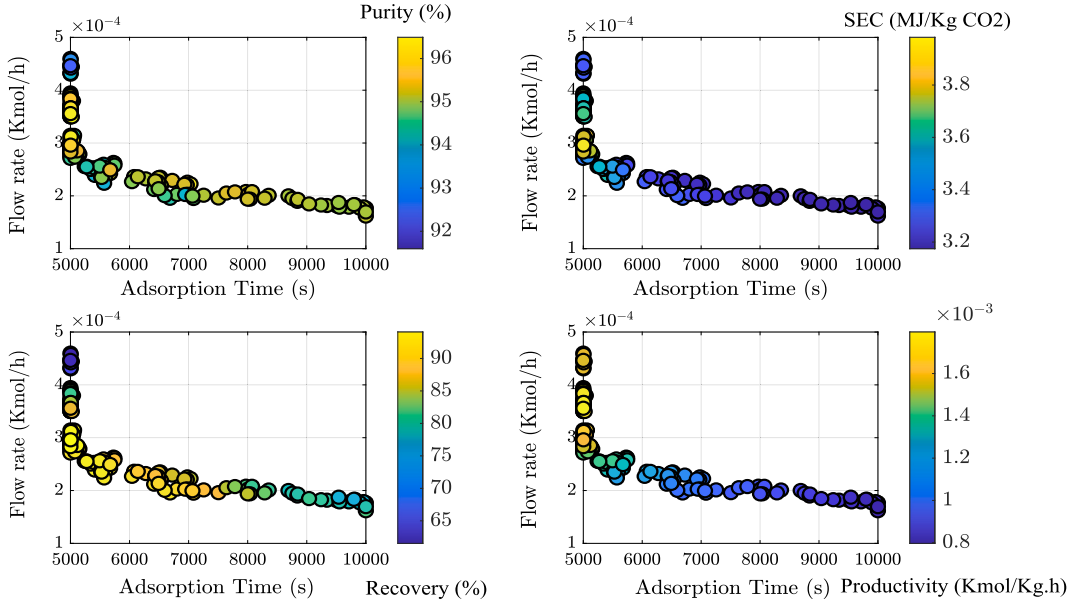

Fig. 19. Effect of flow rate and adsorption time for all four performance indicators.

properly. However, once the temperature exceeds this threshold, further increases within the 120–150 °C range have a limited impact on key performance indicators. Nonetheless, the optimisation results suggest that achieving high productivity and recovery still requires operating at the upper end of this temperature range, in conjunction with adjustments to other decision variables. A similar pattern was observed for the feed temperature. Although the initial exploration range for feed temperature was between 5 and 28 °C, the optimiser focused on a narrow range of 5 to 8 °C, with most optimal designs found between 5 and 6 °C. This indicates that feed temperature plays a crucial role in sorbent performance, with lower temperatures enhancing efficiency- consistent with the trends observed in sensitivity analysis. It is important to note that, in all the discussed designs, CO_2 purity ranges from 94 % to 96.5 %, as illustrated in Fig. 15.

3.4. Optimal design discussion

The two-dimensional Pareto front showing the relationship between CO_2 recovery and SEC is presented in Fig. 20, with the productivity of each Pareto solution indicated by colour. Three distinct regions can be identified based on the range of productivity and SEC. Region 1, Region 2, and Region 3. These regions represent different sets of optimal process designs, each offering a unique balance of performance trade-offs. Importantly, no single region is universally superior; rather, each

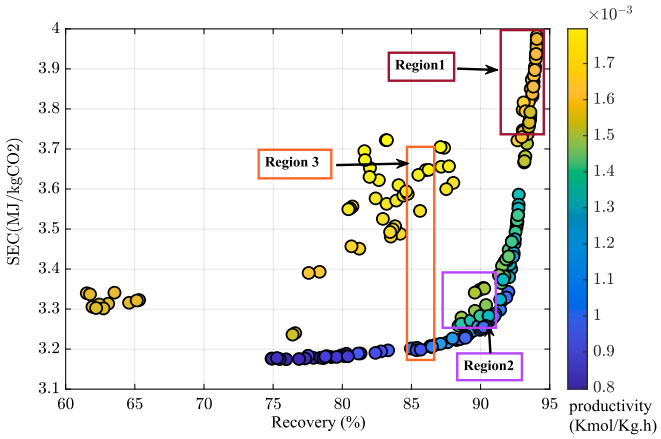

Fig. 20. Two-dimensional Pareto front illustrating the trade-off between SEC and recovery, with productivity represented by colour.

reflects a viable optimal solution depending on specific process priorities. Each design corresponds to a specific combination of operating parameters and cycle configurations. Region 1 is characterised by high productivity (1.6e-3–1.7e-3 Kmol/kg.h), the highest recovery (over 93 %), and the greatest SEC (exceeding 3.7 MJ/kg CO_2). A representative design in this region operates at the maximum heating temperature (150 °C) to enhance sorbent regeneration, combined with a low vacuum pressure (0.07 bar) to facilitate CO_2 desorption by reducing its partial pressure. The cycle employs a short adsorption (5000 s) and desorption time (200 s), which helps shorten the overall cycle and improve productivity. Additionally, the feed temperature is kept at the lowest tested value (5 °C) to increase the sorbent's CO_2 uptake capacity, and a moderate feed flow rate of 2.89 e-4 Kmol/h is applied to ensure adequate CO_2 delivery during the brief adsorption phase. This configuration reflects a design that maximises productivity, recovery, and purity, but demands significantly higher energy input, resulting in elevated SEC.

In contrast, Region 2 achieves relatively high recovery rates (88–92 %) and productivity values ranging from 1.3e-3 to 1.5e-3 Kmol/kg.h, with SEC varying between 3.25 and 3.4 MJ/kg CO_2 depending on the operational conditions. As evident from the reported operational variables for one example from this region, the air enters the adsorption bed at a low temperature of 5 °C to enhance CO_2 capture, while the desorption step requires the highest heating temperature of around 150 °C to effectively regenerate the sorbent. However, this design uses a higher vacuum pressure (0.146 bar) compared to region 1(0.07 bar), which is less energy-intensive for vacuum generation. To compensate for the reduced driving force at this pressure, the system relies on longer desorption (785 s) and adsorption time of 5570 s. This configuration allows the optimiser to balance performance with energy efficiency by selecting conditions that reduce SEC, even if it requires extended cycle durations.

An important aspect of this plot is Region 3, which differs noticeably from the other regions. Within Region 3, two distinct groups of data emerge, each exhibiting different ranges of productivity and SEC while maintaining a constant recovery level. The blue colour group shows productivity between 0.8 e-3 and 1.1e-3 Kmol/kg. s with SEC below 3.2 MJ/kg CO_2, whereas the yellow group achieves the highest productivity values (1.7e-3-1.8e-3 Kmol/kg.h) but with increased SEC ranging from 3.4 to 3.7 MJ/kg CO_2. Examining two representative points from these groups at a constant recovery of 85 % reveals that both require the lowest feed temperature(5 °C) and highest heating temperature (150 °C). However, their other decision variables differ significantly. For the design with lower energy consumption (3.2 MJ/kg CO_2) and moderate productivity of 0.9 e-3 Kmol/kg.h, a lower vacuum pressure (0.15 bar, the minimum considered in this study) is used. To maintain the constant recovery at this vacuum pressure, the adsorption and desorption times need to be extended to 8000 s and 970 s, respectively, while the feed flow rate is reduced to 1.93e −4 Kmol/h. In contrast, increasing productivity at the same recovery level involves raising the vacuum pressure slightly to 0.092 bar and reducing adsorption and desorption

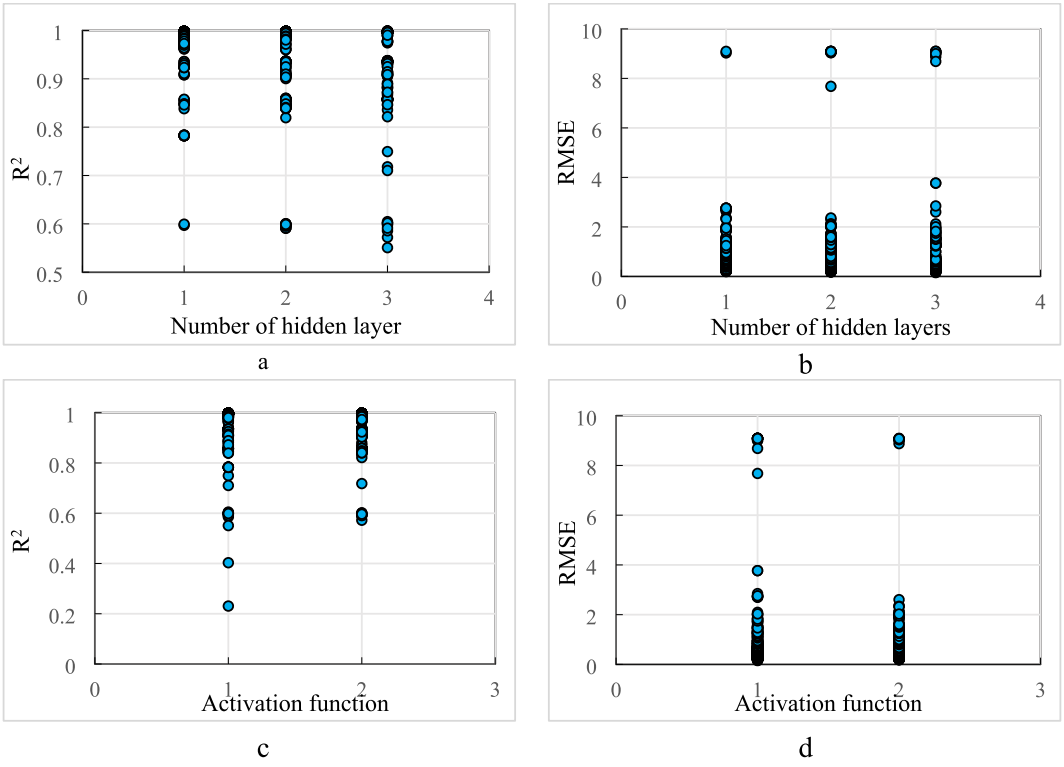

Fig. 9. (a) and (b) Comparison of R^2 and RMSE values for different numbers of hidden layers (1, 2, 3 represent the number of hidden layers), respectively. (c) and (d) Comparison of R2 and RMSE values for selecting the activation function, where option1 represents the tansig function and option 2 represents the logsig function.

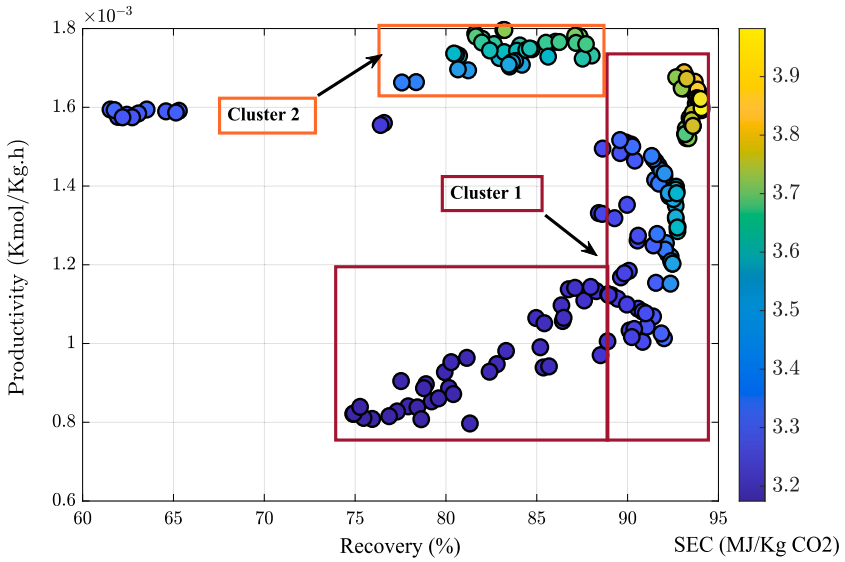

Fig. 16. Two dimensional Pareto front for recovery and productivity.

Table 3
values of error metrics (R^2,MSE, and AARD) of the ANN model for four process performance indicators (SEC, CO_2 purity, recovery, and productivity) across training, validation, and test datasets.

Process parameters	Unit	Training			Validation			Testing		
		R2	MSE	AARD	R2	MSE	AARD	R2	MSE	AARD
SEC	MJ/kg CO_2	0.994	0.004	1.32 %	0.995	0.004	1.32 %	0.994	0.004	1.35 %
CO_2 purity	%	0.936	1.444	0.26 %	0.997	0.078	0.21 %	0.997	0.061	0.18 %
Recovery	%	0.999	0.416	0.76 %	0.999	0.279	0.71 %	0.999	0.232	0.68 %
Productivity	Kmol/kg.h	0.998	0	1.03 %	0.998	0	0.98 %	0.998	0	1.04 %

Table 4
Error comparison of the ANN on the new dataset for four performance indicators: SEC, CO_2 purity, productivity, and recovery.

Process parameters	Unit	R^2	AARD(%)
SEC	MJ/kg CO_2	0.958455	1.6277
CO_2 purity	%	0.990575	0.124495
Productivity	Kmol/kg.h	0.96951	1.69055
Recovery	%	0.87523	1.2468

Table 5
NGSA-II parameters used in this study.

NSGA-II parameters	Quantity
Population	250
Generation	1000
Cross over probability	0.9
Mutation probability	0.1
Cross over index	20
Mutation index	20

time to their minimum values of 5000 and 200 s, respectively, with a higher feed flow rate of 3.55 e-4 Kmol/h. Since productivity depends strongly on time, shorter cycle times boost productivity but increase energy consumption. Therefore, the selection of operating conditions within region 3 depends on whether priority is given to maximising productivity or minimising energy use.

Taking into account the importance of energy usage within Europe, this study recommended designs that prioritise minimising energy consumption while maintaining high recovery and productivity, along with CO_2 purity above 94 %. Therefore, Region 2 is selected, and the results of a representative point from this region are compared with our

Table 6
Comparison of performance indicators for the base case, the recommended optimal case, and the Climeworks reports.

Performance parameters	Unit	Base design	Recommended optimal design	Climeworks
SEC	MJ/kg CO_2	3.85	3.35	6.12–8.18
CO_2 purity	%	98.13	95.3	99.9
Productivity	Kmol/kg.h	3.61e-4	1.5e-3	—
Recovery	%	53.26	90.2	85.4
Reference			This work	[53,54]

Table 7
Comparison of operating conditions between the base case and the recommended optimal case.

Decision variables	Unit	Base design	Recommended optimal design
Feed flow rate	Kmol/h	0.0003	0.000295
Feed temperature	^{0}C	23	5
Heating temperature	^{0}C	150	149.5
Adsorption time	s	7200	5000
Desorption time	s	10,000	504
Vacuum pressure	Bar	0.09	0.127

baseline design. Table 6 compares the performance outcomes of the recommended design against the base case and reported data from Climeworks, while Table 7 represents the values of decision variables for both the base case and the recommended design. As shown, the recommended design achieves notably higher productivity and CO_2 recovery, along with the reduction in SEC, at the expense of a slight drop in

purity from 98 % to 95 %. When compared to the Climeworks reported performance for an unspecified amine-functionalised solid sorbent, the proposed design demonstrates superior productivity, higher recovery, and a reduction in SEC by at least 82 %, albeit with a decrease in CO_2 purity from 99.9 to 95.3 %. This discrepancy is expected, as the current model represents an idealised and optimised system. In contrast to real-world operations, it assumes full sorbent utilisation, negligible pressure drop, and ideal equipment. It also simplifies the process by assuming axial flow through a thin sorbent layer – reducing flow resistance- and neglects energy requirements for water- CO_2 separation. These idealisations contribute to the lower energy consumption observed in the model compared to actual systems like Climeworks.

4. Conclusion

A TVSA cycle model, developed in Aspen Adsorption for capturing CO_2 under DAC conditions using mmen-Mg_2(dobpdc), was employed to optimise the process with the goal of achieving high-purity CO_2 removal, while minimising SEC and maximising both recovery and productivity. Given the computational intensity of the optimisation process – which requires thousands of simulation runs and results in long computation times - a surrogate modelling approach was implemented to identify an optimal design at a reduced computational cost. In particular, an ANN model was developed and integrated with the NSGA-II to efficiently optimise key process variables (Adsorption time, desorption time, adsorption temperature, and vacuum pressure) and feed properties (feed temperature and feed flow rate). To train a high-performance ANN model, 2500 data points were generated using the LHS sampling technique from the detailed simulation model. After validating and testing the Network, a final verification was performed using 300 additional data points. The ANN predictions for these new points were compared against results from the full simulation model to confirm the accuracy of the surrogate model. By integrating the ANN surrogate model and the NSGA-II algorithm, optimal TVSA designs were successfully identified with significantly reduced computation time. Using the same NSGA-II configuration—including 1000 generations and a population of 250, the optimisation with the surrogate model required only approximately 2 h, compared to approximately 350 days if performed directly in Aspen Adsorption, assuming an average of 2-min runtime per dynamic simulation($250 \times 1000 \times 2 = 500{,}000$ min). The developed surrogate model effectively captures complex, nonlinear relationships between process variables and performance outcomes-thereby enhancing optimisation efficiency and enabling faster, more efficient optimisation iterations, ultimately accelerating the discovery of advanced CO_2 capture materials.

Considering the CO_2 purity over 95 %, the resulting Pareto front analysis reveals two distinct data trends, both highlighting a trade-off between SEC and recovery and productivity. In one of these trends, it is observed that under constant recovery, increasing SEC can lead to a significant gain in productivity. Depending on the specific priorities of an industry, whether to maximise throughput or minimise energy consumption, these results offer flexible design options that balance operational efficiency with energy demand. Furthermore, the optimisation results indicate that environmental conditions, particularly ambient temperature (feed temperature), play a critical role in performance. Lower feed temperatures enhance adsorption capacity, thereby increasing recovery, and making ambient temperature an important factor in achieving optimal TVSA operation for this sorbent.

The insights gained from this study demonstrate the potential application of mmen-Mg_2(dobpdc) in industrial DAC systems. For future work, we aim to upscale the model to the industrial scale to evaluate the performance of this sorbent under realistic operating conditions. Additionally, considering the effect of humidity is essential, as water in the air can significantly influence CO_2 adsorption behaviour; incorporating this factor will improve the reliability of predictions and guide practical DAC implementation. These steps will help bridge the gap between lab-scale optimisation and industrial deployment, providing a more comprehensive understanding of the sorbent's performance in real-world DAC operations.

Finally, Comprehensive climate mitigation demands that we complement capture technologies with cleaner transition energy fuels. Natural gas remains a vital bridge in this energy matrix, necessitating continued rigour in extraction mechanics, specifically the flowback and cleanup processes that govern unconventional reservoir performance [55–57].

CRediT authorship contribution statement

Maryam Nasiri-ghiri: Writing – review & editing, Writing – original draft, Visualization, Validation, Software, Methodology, Investigation, Formal analysis, Data curation, Conceptualization. **Hamid Reza Nasriani:** Writing – review & editing, Visualization, Supervision, Resources, Project administration, Investigation, Funding acquisition, Conceptualization. **Leila Khajenoori:** Writing – review & editing, Supervision, Resources, Investigation, Funding acquisition, Conceptualization. **Samira Khani Rasmussen:** Writing – review & editing, Supervision, Investigation, Funding acquisition, Formal analysis, Conceptualization. **Karl Williams:** Writing – review & editing, Supervision, Resources, Formal analysis, Conceptualization.

Declaration of competing interest

The authors declare that they have no known competing financial interests or personal relationships that could have appeared to influence the work reported in this paper.

Appendix A. Supplementary data

Supplementary data to this article can be found online at https://doi.org/10.1016/j.seppur.2025.136177.

Data availability

Data will be made available on request.

References

[1] X.T.P.K. W. T. Lan, "Trends in globally-averaged CO2 determined from NOAA Global Monitoring Laboratory measurements,", https://gml.noaa.gov/ccgg/trends/global.html#global.
[2] IEA, CO2 emissions in 2023. https://www.iea.org/reports/co2-emissions-in-2023, 2024 [Online]. Available, https://www.iea.org/reports/clean-energy-market-monitor-march-2024.
[3] Theo Stein, "No sign of greenhouse gases increases slowing in 2023," Apr. 2024. Accessed: Apr. 05, 2024. [Online]. Available, https://research.noaa.gov/no-sign-of-greenhouse-gases-increases-slowing-in-2023/.
[4] M. Ozkan, R. Custelcean, The status and prospects of materials for carbon capture technologies, MRS Bull. 47 (4) (2022) 390–394, https://doi.org/10.1557/s43577-022-00364-9.
[5] UNFCCC, "Key aspects of the Paris Agreement," https://unfccc.int/. [Online]. Available, https://unfccc.int/.
[6] K. Lackner, A. Hans-Joachim Ziock, P. Grimes, and G. Associates, Carbon Dioxide Extraction From &r: Is It An Option?, in: Los a: 24th Annual Technical Conference on Coal Utilization and Fuel Systems, Clearwater, 1999. Accessed: Feb. 01, 1999. [Online]. Available: https://www.osti.gov/biblio/770509.
[7] F.J. Medaiyese, H.R. Nasriani, L. Khajenoori, K. Khan, A. Badiei, From Waste to Energy: Enhancing Fuel and Hydrogen Production through Pyrolysis and In-Line Reforming of Plastic Wastes, Multidisciplinary Digital Publishing Institute (MDPI). (2024), https://doi.org/10.3390/su16124973.
[8] F. Barzagli, M. Peruzzini, R. Zhang, Screening study on the performance of different amine systems for direct CO 2 capture from air [Online]. Available: https://ssrn.com/abstract=5010492, 2024.
[9] F. Barzagli, C. Giorgi, F. Mani, M. Peruzzini, Screening study of different amine-based solutions as sorbents for direct CO2Capture from air, ACS Sustain. Chem. Eng. 8 (37) (2020) 14013–14021, https://doi.org/10.1021/acssuschemeng.0c03800.
[10] F. Sabatino, M. Gazzani, F. Gallucci, M. van Sint Annaland, Modeling, optimization, and techno-economic analysis of bipolar membrane Electrodialysis

for direct air capture processes, Industrial & Engineering Chemistry Research 61 (34) (2022) 12668–12679, https://doi.org/10.1021/acs.iecr.2c00889.
[11] H. Ted Von, Thermal removal of carbon dioxide from the atmosphere: energy requirements and scaling issue, Clim. Change 148 (2018) 491–501.
[12] C. Song, Q. Liu, N. Ji, S. Deng, J. Zhao, Y. Kitamura, Advanced cryogenic CO2 capture process based on Stirling coolers by heat integration, Appl. Therm. Eng. 114 (2017) 887–895, https://doi.org/10.1016/J.APPLTHERMALENG.2016.12.049.
[13] M. Aghaie, N. Rezaei, S. Zendehboudi, A systematic review on CO2 capture with ionic liquids: Current status and future prospects, Elsevier Ltd. (2018), https://doi.org/10.1016/j.rser.2018.07.004.
[14] R.M. Firdaus, A. Desforges, A. Rahman Mohamed, B. Vigolo, Progress in adsorption capacity of nanomaterials for carbon dioxide capture: a comparative study, J. Clean. Prod. 328 (2021) 129553, https://doi.org/10.1016/J.JCLEPRO.2021.129553.
[15] A. Allangawi, et al., Carbon Capture Materials in Post-Combustion: Adsorption and Absorption-Based Processes, Multidisciplinary Digital Publishing Institute (MDPI). (2023), https://doi.org/10.3390/c9010017.
[16] J. Elfving, C. Bajamundi, J. Kauppinen, T. Sainio, Modelling of equilibrium working capacity of PSA, TSA and TVSA processes for CO2 adsorption under direct air capture conditions, J. CO_2 Util. 22 (2017) 270–277, https://doi.org/10.1016/j.jcou.2017.10.010.
[17] M. Gholami, T.R. Van Assche, J.F. Denayer, Temperature vacuum swing, a combined adsorption cycle for carbon capture, Elsevier Ltd. (2023), https://doi.org/10.1016/j.coche.2022.100891.
[18] D. Marinič, B. Likozar, Direct air capture multiscale modelling: From capture material optimization to process simulations, Elsevier Ltd. (2023), https://doi.org/10.1016/j.jclepro.2023.137185.
[19] W. Liu, Y.C. Lin, Y. Ji, J.Y. Yong, X.J. Zhang, L. Jiang, Thermodynamic study on two adsorption working cycles for direct air capture, Appl. Therm. Eng. 214 (2022), https://doi.org/10.1016/j.applthermaleng.2022.118920.
[20] S. Li, et al., Cyclic performance evaluation of CO2 adsorption using polyethylene terephthalate plastic-waste-derived activated carbon, Fuel 331 (2023) 125599, https://doi.org/10.1016/J.FUEL.2022.125599.
[21] J.A. Wurzbacher, C. Gebald, N. Piatkowski, A. Steinfeld, Concurrent separation of CO2 and H2O from air by a temperature-vacuum swing adsorption/desorption cycle, Environ. Sci. Technol. 46 (16) (2012) 9191–9198, https://doi.org/10.1021/es301953k.
[22] X. Zhu, T. Ge, F. Yang, R. Wang, Design of steam-assisted temperature vacuum-swing adsorption processes for efficient CO2 capture from ambient air, Renew. Sustain. Energy Rev. 137 (2021) 110651, https://doi.org/10.1016/J.RSER.2020.110651.
[23] Q. Zhang, S. Deng, R. Zhao, B. Zhang, Multi-optimization of carbon capture by temperature swing adsorption based on artificial neural network surrogate model, 2025.
[24] K. Deb, Multi-objective optimisation using evolutionary algorithms: An introduction, in: Multi-Objective Evolutionary Optimisation for Product Design and Manufacturing, Springer, London, 2011.
[25] K. Agrawal, S. Pratap, A. Meyarivan, T. Deb, A Fast Elitist Non-dominated Sorting Genetic Algorithm for Multi-Objective Optimization: NSGA-II, Springer, Berlin, Heidelberg, 2000.
[26] J. Knowles, D. Corne, "The Pareto archived evolution strategy: a new baseline algorithm for Pareto multi objective optimisation," in Proceedings of the 1999 Congress on Evolutionary Computation-CEC99, Washington: IEEE, Aug, 1999, pp. 98–105.
[27] E. Thiele, L. Zitzler, "Multiobjective optimization using evolutionary algorithms — A comparative case study," in A comparative case study. In: Eiben, A.E., Bäck, T., Schoenauer, M., Schwefel, HP. (eds) Parallel Problem Solving from Nature, A. E., 'Bäck, T. ', 'Schoenauer, M. ', 'Schwefel, H. (eds) P. P. S. from N. 'Eiben, Ed., Berlin: Springer, 1998, pp. 292–301.
[28] S. Verma, M. Pant, V. Snasel, A comprehensive review on NSGA-II for multi-objective combinatorial optimization problems, IEEE Access 9 (2021) 57757–57791, https://doi.org/10.1109/ACCESS.2021.3070634.
[29] S. Krishnamurthy, et al., Simulation and optimization of fixed bed and moving bed TSA processes for post-combustion CO2 capture, Computer Aided Chemical Engineering 52 (2023) 313–318, https://doi.org/10.1016/B978-0-443-15274-0.50050-0.
[30] M. Bagheri, M. Fakhroleslam, S. Fatemi, Ultra-dilute CO2 capture in an ethane treatment plant via temperature swing adsorption: simulation-based analysis and multi-objective optimal design, Sep. Purif. Technol. 356 (2025) 129968, https://doi.org/10.1016/J.SEPPUR.2024.129968.
[31] J. Du, et al., Development of hybrid surrogate model structures for design and optimization of CO2 capture processes: part I. Vacuum pressure swing adsorption in a confined space, Chem. Eng. Sci. 283 (2024) 119379, https://doi.org/10.1016/J.CES.2023.119379.
[32] G. Yongchul, G.C. Seongbin, Recent advances in software tools for adsorption science and engineering, Molecular System Design & Engineering 7 (2022) 686–701.
[33] Lisa JossMatteo GazzaniMax HeftiDorian MarxMarco Mazzotti, Temperature swing adsorption for the recovery of the heavy component: an equilibrium-based shortcut model, Ind Eng Chem Res 54 (11) (2015) 3027–3038.
[34] B.J. Maring, P.A. Webley, A new simplified pressure/vacuum swing adsorption model for rapid adsorbent screening for CO2 capture applications, Int. J. Greenh. Gas Con. 15 (2013) 16–31, https://doi.org/10.1016/J.IJGGC.2013.01.009.
[35] R. Zhao, L. Liu, L. Zhao, S. Deng, S. Li, Y. Zhang, A comprehensive performance evaluation of temperature swing adsorption for post-combustion carbon dioxide capture, Renew. Sustain. Energy Rev. 114 (2019) 109285, https://doi.org/10.1016/J.RSER.2019.109285.
[36] J. Young, F. Mcilwaine, B. Smit, S. Garcia, M. van der Spek, Process-informed adsorbent design guidelines for direct air capture, Chem. Eng. J. 456 (2023), https://doi.org/10.1016/j.cej.2022.141035.
[37] D.A. Pisner, D.M. Schnyer, Support vector machine, Machine Learning: Methods and Applications to Brain Disorders (2020) 101–121, https://doi.org/10.1016/B978-0-12-815739-8.00006-7.
[38] M. Buhmann, Radial basis functions. Acta Numerica. 2000;9:1–38, 2001.
[39] R.M. Neuwirth, E. Heiberger, Polynomial Regression, in: Mathematics and Statistics Mathematics and Statistics (R0), Springer, New York, NY, 2009.
[40] M.Y. Rafiq, G. Bugmann, D.J. Easterbrook, Neural network design for engineering applications, Comput. Struct. 79 (17) (2001) 1541–1552, https://doi.org/10.1016/S0045-7949(01)00039-6.
[41] P. Boyle, Gaussian Processes for Regression and Optimisation, University of Wellington, 2007.
[42] S.G. Subraveti, Z. Li, V. Prasad, A. Rajendran, Machine learning-based multiobjective optimization of pressure swing adsorption, Ind Eng Chem Res 58 (44) (2019) 20412–20422, https://doi.org/10.1021/acs.iecr.9b04173.
[43] M.N. Ghiri, H.R. Nasriani, L. Khajenoori, S. Mohammadkhani, K.S. Williams, Dynamic Temperature–Vacuum Swing Adsorption for Sustainable Direct Air Capture: Parametric Optimisation for High-Purity CO2 Removal, Sustainability 17 (15) (2025) 6796, https://doi.org/10.3390/su17156796.
[44] L.A. Darunte, et al., Moving beyond adsorption capacity in Design of Adsorbents for CO 2 capture from Ultradilute feeds: kinetics of CO 2 adsorption in materials with stepped isotherms, Ind. Eng. Chem. Res. 58 (1) (2019) 366–377, https://doi.org/10.1021/acs.iecr.8b05042.
[45] A. Lalit, D. DaruntеAloysius, S. OetomoKrista, S. Walton David, Sholl Christopher W. Jones, Direct air capture of CO2 using amine functionalized MIL-101(Cr), ACS Sustain Chem Eng 4 (10) (2016) 5761–5768.
[46] M.D.A. Beckman, R.J.A. Conover, W.J. McKay, A comparison of three methods for selecting values of input variables in the analysis of output from a computer code, Technometrics 42 (1) (2000) 55–61.
[47] Y. Shichkina, Y. Irishina, E. Stanevich, A. de Jesus Plasencia, Salgueiro, Application of genetic algorithms for the selection of neural network architecture in the monitoring system for patients with parkinson's disease, Appl. Sci. (Switz.) 11 (12) (2021), https://doi.org/10.3390/app11125470.
[48] Z. Wang, Y. Shen, D. Zhang, Z. Tang, W. Li, A comparative study of multi-objective optimization with ANN-based VPSA model for CO2 capture from dry flue gas, J. Environ. Chem. Eng. 10 (3) (2022) 108031, https://doi.org/10.1016/J.JECE.2022.108031.
[49] J. Bilbao Bilbao, Overfitting problem and the over-training in the era of data: Particularly for Artificial Neural Networks, in: Eighth International Conference on Intelligent Computing and Information Systems (ICICIS), Cairo. Egypt, 2017, pp. 173–177.
[50] X. Chenglong, L. Liang, F. Pascal, B. Michael, W. Pierre, B.R.C. Jinsheng, Machine learning–based optimization for hydrogen purification performance of layered bed pressure swing adsorption, Int. J. Energy Res. 44 (6) (2020) 4475–4492.
[51] K. Deb, M. Goyal, Optimizing Engineering Designs Using a Combined Genetic Search, 2025.
[52] S. Kumar, V. Sharma, A comprehensive review on multi-objective optimization techniques: past, present and future, Archives of Computational Methods in Engineering 29 (2022) 5605–5633.
[53] F. Olga, E. Christian, B. Mahdi, Techno-economic assessment of CO2 direct air capture plants, J. Clean. Prod. 224 (2019) 957–980.
[54] S. Bardow, A. Deutz, Life-cycle assessment of an industrial direct air capture process based on temperature–vacuum swing adsorption, Nat Energy 6 (2021) 203–213.
[55] H.R. Nasriani, M. Jamiolahmady, Flowback cleanup mechanisms of post-hydraulic fracturing in unconventional natural gas reservoirs, J. Nat. Gas Sci. Eng. 66 (2019) 316–342.
[56] H.R. Nasriani, M. Jamiolahmady, T. Saif, J. Sánchez, A systematic investigation into the flowback cleanup of hydraulic-fractured wells in unconventional gas plays, Int. J. Coal Geol. 193 (2018) 46–60.
[57] H.R. Nasriani, M. Jamiolahmady, Maximizing fracture productivity in unconventional fields; analysis of post hydraulic fracturing flowback cleanup, J. Nat. Gas Sci. Eng. 52 (2018) 529–548.